An International Journal of Optimization and Control: Theories & Applications
ISSN: 2146-0957 eISSN: 2146-5703
Vol. 16, No. 2, pp.752-773 (2026)
https://doi.org/10.36922/IJOCTA025500226

RESEARCH ARTICLE

Finite-time boundedness synthesis for Bouc–Wen hysteresis dynamic systems using non-fragile event-triggered Takagi–Sugeno fuzzy control

Arumugam Arunkumar[1], Jenq-Lang Wu[2], Wen-Jer Chang[1*], and Yann-Horng Lin[1]

[1] Department of Marine Engineering, National Taiwan Ocean University, Keelung, Taiwan, China
[2] Department of Electrical Engineering, National Taiwan Ocean University, Keelung, Taiwan, China
arunapm@yahoo.com;wujl@mail.ntou.edu.tw;wjchangntou@gmail.com;ginobili9815318@gmail.com

ARTICLE INFO

Article history:
Received: December 8, 2025
Revised: January 22, 2026
Accepted: January 29, 2026
Published Online: April 2, 2026

Keywords:
Bouc–Wen hysteresis behavior
Event-triggered mechanism
Finite-time boundedness
Non-fragile controller
Fuzzy system

AMS Classification 2010:
26A33; 34A08; 35H15;
34K50 47H10; 60H10

ABSTRACT

This paper investigates the finite-time (FT) control problem for Takagi-Sugeno (T-S) fuzzy Bouc-Wen (B-W) hysteresis systems under a fuzzy event-triggered (ET) non-fragile control framework. A novel T–S fuzzy hysteresis state estimator is developed to estimate the virtual hysteresis state, enabling accurate compensation of hysteresis effects in networked control environments. To reduce communication burden while preserving closed-loop performance, a fuzzy ET mechanism is incorporated into the control architecture, allowing adaptive transmission based on system dynamics. In contrast to existing hysteresis control methods, the proposed scheme integrates a newly developed T–S fuzzy hysteresis model, an ET mechanism, and a non-fragile control design within a unified FT framework. The main objective is to guarantee FT boundedness (FTB) of the closed-loop T–S fuzzy B–W hysteresis system while simultaneously achieving prescribed FT mixed H_∞ and passivity performance indices. By employing the Lyapunov–Krasovskii functional methodology, a set of novel sufficient conditions is derived in terms of linear matrix inequalities, ensuring FTB and the desired performance criteria. The effectiveness and feasibility of the proposed control strategy are validated through three numerical examples.

1. Introduction

The control of dynamical systems exhibiting hysteresis nonlinearities has recently become an important research topic, as such nonlinearities are widely encountered in industrial applications, particularly in actuators based on smart materials, including shape-memory alloys and piezoceramic elements.[1] These hysteresis effects introduce nondifferentiable nonlinearities that significantly complicate controller design, causing performance degradation, undesired oscillations, or even instability in closed-loop systems.[2] Due to their nonsmooth characteristics, traditional control strategies are generally ineffective in mitigating hysteresis-induced effects. According to research findings, the persistence of hysteresis effects necessitates the utilization of advanced control methodologies, which have been the subject of investigation for numerous years. Successfully tackling these challenges requires developing a precise model that captures the nonlinear attributes inherent in hysteresis phenomena, thereby facilitating the design of effective control systems. In pursuit of this goal, various mathematical models have been scrutinized in scholarly works to depict the nonlinearity associated with hysteresis, each exhibiting unique characteristics.[3,4] As an example, the Preisach model employs an integral representation whose kernel determines the form of the hysteresis loop.[5] Conversely, the Duhen model exploits the behavior transformation of

* Corresponding author

the output in response to a change in the input direction.[6] Another approach is based on a nonlinear feedback model, in which a nonlinear feedback map induces multiple attracting equilibrium points.[7] The Bouc–Wen (B–W) model describes hysteresis behavior through a differential equation that relates the input and output.[8,9] Collectively, these models demonstrate the diversity of existing approaches to hysteresis representation. A comprehensive discussion and summary of the characteristics of various hysteresis modeling techniques can be found in Ref. 5.

Among the several approaches to describing hysteresis, the B–W model is widely recognized as a phenomenological model in mechanics, celebrated for its ability to encapsulate hysteresis phenomena.[10] The B–W model uses a nonlinear first-order differential equation to establish a hysteresis relationship between the input and output.[11] Its parameters enable the analytical representation of various hysteretic cycles. The B–W model's utility in characterizing hysteretic behavior has attracted increased attention from researchers, who are investigating its control, stability, and identification properties.[12] Despite this, there has been limited exploration of its application in control systems.[11–14] Furthermore, Flores et al.[11] examined an adaptive-based output feedback controller designed for nonlinear uncertain systems exhibiting B–W type hysteresis nonlinearity. For example, a recent study explored a tracking adaptive control method for nonlinear dynamical systems along with B–W hysteresis, addressing challenges, such as unknown actuator nonlinearity, parametric uncertainty, and bounded external disturbances.[14] Another recent study delved into the state-constrained control problem for hysteresis systems, utilizing the classical B–W model and employing the L_2 gain control approach.[13] However, previous research has only scratched the surface regarding control systems employing B–W hysteresis, as indicated in the studies.[11–15] Our proposed work introduces a significant innovation through the development of a novel Takagi–Sugeno (T–S) fuzzy hysteresis estimator. The estimator is constructed using a detailed model of the controlled system, enabling accurate estimation of the hysteresis state.

The rapid development of control theory and communication network technologies in recent years has led to the emergence of networked control systems (NCSs) as a major interdisciplinary research focus.[15,16] The NCS constitutes a closed-loop feedback system, yet its operational mode differs from conventional point-to-point control systems. It enables cross-regional data exchange by connecting actuators, sensors, and controllers across different zones through a shared multifunctional network.[17] By combining network and physical spaces, NCSs enable remote data access and multitasking capabilities. This fusion provides control systems with numerous advantages, including data sharing, high resource utilization, and reduced installation and maintenance costs.[18] As a result, contemporary NCSs are advancing toward decentralization, intelligence, and structural complexity, and have been widely applied in domains such as industrial automation, smart grids, space missions, and system diagnostics.[19] Moreover, in networked systems, signal transmission relies on communication channels, while limited sensor energy and network bandwidth constrain other communication activities.[20] Consequently, an alternative strategy, the event-triggered (ET) control mechanism, has emerged as a promising solution for networked systems, effectively reducing computational load and communication overhead while ensuring adequate control performance. Within an ET control framework, data transmission occurs only when the current signal exceeds the specified triggering threshold.[21] Several studies have demonstrated that ET control enhances bandwidth efficiency and minimizes energy consumption in networked systems.[22–27] Furthermore, dynamic ET reinforcement learning-based consensus tracking of nonlinear multi-agent systems is studied by Xu et al.[25] In particular, Guo et al.[26] develop a dynamic event-driven adaptive dynamic programming approach for N-player nonzero-sum games, while Pan et al.[27] propose an ET predefined-time control method with command filtering error compensation to improve system performance under full-state constraints. Nevertheless, limited research has been carried out on hysteresis behavior in networked environments.[28–30] For example, in a previous study, an ET control scheme was taken into account while dealing with hysteresis systems using nonlinear hysteresis characteristics and disturbances.[30] A backlash-like unknown hysteresis problem for nonlinear large-scale systems is then discussed, with an ET-based adaptive neural network.

In reality, networked environments often encounter complexity, uncertainty, or vagueness during mathematical modeling.[29] To overcome this shortcoming, the fuzzy approach is considered more suitable. Among different fuzzy techniques, the T–S fuzzy model[18] is a more popular and efficient tool for analyzing and synthesizing complex nonlinear systems, in which a nonlinear plant is approximated and analyzed using the T–S fuzzy linear model. Numerous meaningful contributions

on T–S fuzzy networked systems can be found in the literature.[18,29–31] In particular, the study by Shi et al.[18] examined the ET H_∞control problem for switched T–S fuzzy systems. However, there is no discussion on the control of T–S fuzzy B–W hysteresis systems. Specifically, no fuzzy method has been developed to model the B–W hysteresis behavior. A fuzzy hysteresis model for describing the B–W hysteresis behavior is worth investigating. Compared to traditional hysteresis models, the fuzzy hysteresis model offers several advantages, making it an effective substitute in a wide range of applications. Unlike conventional approaches that rely on predefined mathematical formulations, the fuzzy hysteresis model offers enhanced flexibility by effectively accommodating uncertainties and nonlinearities. This adaptability enables an accurate representation of hysteretic behavior, particularly in complex and dynamic systems. Replacing the traditional hysteresis model with the fuzzy hysteresis model can lead to more reliable and efficient system performance, justifying its adoption in relevant engineering and scientific fields.

In practical applications, hysteresis systems are prone to disturbances that can influence the controller's behavior. Therefore, developing a robust controller that accommodates gain variations during the control process is essential, since such variations may degrade system performance. To overcome this limitation, additional adjustable parameters are introduced in the controller design without impairing system performance. Such controllers are commonly known as non-fragile controllers.[32,33] Recently, non-fragile control design has emerged as an important research direction. Using a non-fragile controller, an observer-based algorithm is proposed by Arunkumar and Wu[34] for the extracorporeal blood circulation process in the finite-time (FT) span. However, there is no discussion on a non-fragile controller for T–S fuzzy B–W hysteresis systems. Despite substantial research on various facets of the B–W hysteresis model, there exists a distinct void in its integration with a non-fragile controller. Addressing this gap, our study introduces a pioneering control strategy that integrates hysteresis behavior via a fuzzy ET mechanism alongside a non-fragile controller. This novel approach not only fills an existing research gap but also offers valuable insights for future studies.

Additionally, FT boundedness (FTB) provides an effective framework in practical control systems for achieving swift transient dynamics. Consequently, considerable attention has been given to the study of FTB, resulting in a wealth of important theoretical and practical findings.[11,19,22,31,34] While numerous studies have investigated the FT consensus problem for various dynamical systems, the simultaneous consideration of H_∞ performance, passivity, and non-fragile control for T–S fuzzy B–W hysteresis systems under ET mechanisms has not been adequately addressed. This challenging and practically relevant issue forms the primary motivation of our study. Motivated by the aforementioned discussion, using the B–W hysteresis input technique, an ET non-fragile control scheme is proposed to ensure the FTB of the T–S fuzzy hysteresis systems. To underscore the significance of this research compared to prior work, the following contributions are highlighted:

- The hysteresis behavior-based fuzzy ET non-fragile controller introduced in this study differs significantly from traditional control methods.[3,4,10–12,14] Unlike conventional approaches, which continuously update the controller's state, the proposed controller updates its state and adjusts the controller only at specific triggering instants, thereby reducing the communication burden. Moreover, the issue of hysteresis input, which has been overlooked in prior works,[15,18,19,29,30] is effectively addressed. Consequently, the innovative fuzzy control scheme presented in this research can efficiently regulate T–S fuzzy systems with B–W hysteresis input within an FT interval under the fuzzy ET non-fragile control framework.
- This study introduces a pioneering controller design, integrating a fuzzy ET mechanism with a non-fragile controller, departing from the hysteresis control systems examined in prior studies.[10–12]
- In comparison with previously published works on T–S fuzzy networked systems,[18,31,35,36] the T–S fuzzy B–W hysteresis systems with an ET non-fragile control are proposed because the B–W hysteresis model can capture the hysteresis phenomenon more accurately than other hysteresis models.
- Moreover, in contrast to the hysteresis control systems examined in prior research,[10,12,28–30] our hysteresis state estimation framework is distinguished by its innovative methodology for accurately estimating the virtual hysteresis state.
- By employing appropriately chosen Lyapunov functions and the linear matrix inequality (LMI) approach, we have developed a new set of criteria to meet the necessary FTB criterion while ensuring a prescribed FT mixed H_∞ and

passivity performance index within a B–W hysteresis system.

Finally, three practical numerical examples are showcased to underscore the efficacy of the proposed control methodology.

2. Problem formulation and preliminaries

2.1. System Information

This article addresses an ET non-fragile control design challenge for a specific class of T–S Fuzzy B–W hysteresis systems illustrated in **Figure 1**. To conserve limited network resources, an ET generator is deployed at each sensor node. In consideration of the aforementioned issue and employing T–S fuzzy modeling, the differential equation describing B–W hysteresis systems with the η^{th}, $\eta \in \{1, 2, \ldots, r\}$, fuzzy rule is depicted below (**Equations 1 and 2**):

Plant Rule η : IF $f_1(x)$ *is* $F_{1\eta}$ and $f_2(x)$ *is* $F_{2\eta}$ and ... and $f_q(x)$ *is* $F_{q\eta}$ THEN

$$\dot{x} = A_\eta x + B_\eta H(u) \tag{1}$$

$$z = D_\eta x \tag{2}$$

where $\{f_1(x), f_2(x), \cdots, f_q(x)\}^{\mathrm{T}}$ specifies the premise variables; $F_{j\eta}$ with $(j = 1, 2, \cdots, q,\ \eta = 1, 2, \cdots,\ r)$ denotes the fuzzy rule coefficients. The vector $x \in \mathbb{R}^n$ represents the state of the system, while $u \in \mathbb{R}$ indicates the ideal control input generated by the controller. Additionally, $v = H(u) \in \mathbb{R}$ denotes the actual control force generated by the actuator due to the hysteresis effect, and $z \in \mathbb{R}^s$ represents the controlled output. The system involves known constant matrices $A_\eta \in \mathbb{R}^{n\times n}$, $B_\eta \in \mathbb{R}^n$, and $D_\eta \in \mathbb{R}^{s\times n}$.

If we define $\lambda_\eta(f(x))$ as the normalized membership function corresponding to the inferred fuzzy set $\beta_\eta(f(x))$, the defuzzified structure of T–S fuzzy B–W hysteresis systems, in light of the preceding discussions, can be rephrased as Equations 3 and 4:

$$\dot{x} = \sum_{\eta=1}^{r} \lambda_\eta(f(x)) \{A_\eta x + B_\eta H(u)\} \tag{3}$$

$$z = \sum_{\eta=1}^{r} \lambda_\eta(f(x)) \{D_\eta x\} \tag{4}$$

where $\lambda_\eta(f(x)) = \frac{\beta_\eta(f(x))}{\sum_{\eta=1}^{r}\beta_\eta(f(x))}$ in which $\beta_\eta(f(x)) = \prod_{j=1}^{q} F_{j\eta}(f_j(x))$, here $F_{j\eta}(f_j(x))$ indicates the grade of the membership function of $f_j(x)$ in $F_{j\eta}$. Hence, $\lambda_\eta(f(x))$ satisfy $\lambda_\eta(f(x)) \geq 0$ and $\sum_{\eta=1}^{r}\lambda_\eta(f(x)) = 1$.

2.2. Takagi–Sugeno fuzzy-based Bouc–Wen hysteresis model

A novel fuzzy hysteresis model enables the design of controllers that can effectively accommodate complex, nonlinear behaviors while ensuring stability and performance. It serves as a powerful tool for accurately modeling and controlling systems that exhibit hysteresis behavior, thereby enhancing performance and robustness in practical applications.

In this paper, the fuzzy B–W hysteresis state is governed by the following first-order differential equation under the ζ^{th} fuzzy rule (Equations 5 and 6):

Hysteresis Rule ζ : IF $f_1(x)$ *is* $F_{1\zeta}$ and $f_2(x)$ *is* $F_{2\zeta}$ and ... and $f_q(x)$ *is* $F_{q\zeta}$ THEN

$$\dot{\varsigma} = \dot{u} - \beta_\zeta |\dot{u}| \, |\varsigma|^{r-1}\varsigma - \chi_\zeta \dot{u}|\varsigma|^r \tag{5}$$

$$v = H(u) = \mu_{1\zeta} u + \mu_{2\zeta}\varsigma \tag{6}$$

where $\mu_{1\zeta} > 0$ and $\mu_{2\zeta} > 0$ represent the parameters of hysteresis, the variable $\varsigma \in \mathcal{R}$ is an auxiliary virtual variable that denotes the hysteresis state, and the parameters β_ζ, χ_ζ, and r, are parameters governing the shape and intensity of the hysteresis effect. We assume $\beta_\zeta > |\chi_\zeta|$ and $r \geq 1$. Based on the findings presented in a previous study, it has been demonstrated that the solution ς of Equation 6 not only remains bounded but also fulfills the following criteria (Equation 7)[9]:

$$|\varsigma(t)| \leq \sum_{\zeta=1}^{r} \lambda_\zeta(f(x)) \sqrt[r]{\frac{1}{\beta_\zeta + \chi_\zeta}} \tag{7}$$

Then, the defuzzified output of the T–S fuzzy-based B–W hysteresis dynamics can be inferred as follows (Equation 8)):

$$\dot{x} = \sum_{\eta=1}^{r}\sum_{\zeta=1}^{r} \lambda_\eta(f(x)) \lambda_\zeta(f(x)) \times \{A_\eta x + B_\eta(\mu_{1\zeta}u + \mu_{2\zeta}\varsigma)\}$$

$$\dot{\varsigma} = \sum_{\zeta=1}^{r} \lambda_\zeta(f(x)) \left\{\dot{u} - \beta_\zeta |\dot{u}| \, |\varsigma|^{r-1}\varsigma - \chi_\zeta \dot{u}|\varsigma|^r\right\} \tag{8}$$

$$z = \sum_{\eta=1}^{r} \lambda_\eta(f(x)) \{D_\eta x\}$$

2.3. Takagi-Sugeno fuzzy hysteresis estimator

To establish the control law, we must compensate for the impact of ς, noting that it is a virtual state and thus not accessible for direct feedback. In this

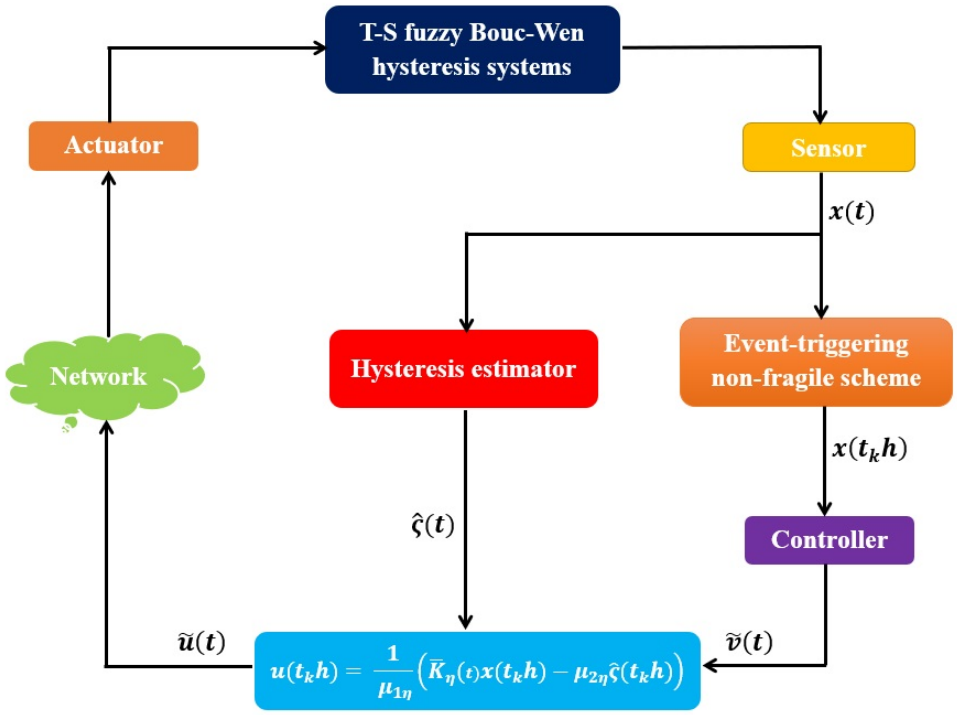

Figure 1. Architecture of the event-triggered non-fragile scheme for Takagi–Sugeno (T–S) fuzzy Bouc–Wen hysteresis systems

regard, we introduce a new method for estimating it and subsequently adjusting for it when designing controllers. In the proposed work, we present a practical and efficient strategy for estimating the hysteresis state ς, across all potential values of r.

From Equation 8, we can derive Equation 9:

$$\sum_{\eta=1}^{r}\sum_{\zeta=1}^{r}\lambda_\eta\left(f\left(x\right)\right)\lambda_\zeta\left(f\left(x\right)\right)\left\{B_\eta\left(\mu_{1\zeta}u+\mu_{2\zeta}\varsigma\right)\right\}$$
$$=\sum_{\eta=1}^{r}\sum_{\zeta=1}^{r}\lambda_\eta\left(f\left(x\right)\right)\lambda_\zeta\left(f\left(x\right)\right)\left\{\dot{x}-A_\eta x\right\} \quad (9)$$

Premultiplying both sides of Equation 9 by B_η^T, Equation 10 is obtained:

$$\sum_{\eta=1}^{r}\sum_{\zeta=1}^{r}\lambda_\eta\left(f\left(x\right)\right)\lambda_\zeta\left(f\left(x\right)\right)$$
$$\times\left\{\mu_{1\zeta}\|B_\eta\|^2u+\mu_{1\zeta}\|B_\eta\|^2\varsigma\right\}$$

$$=\sum_{\eta=1}^{r}\sum_{\zeta=1}^{r}\lambda_\eta\left(f\left(x\right)\right)\lambda_\zeta\left(f\left(x\right)\right)\left\{B_\eta^T\dot{x}-B_\eta^TA_\eta x\right\} \quad (10)$$

Thus, we can determine ς using the following approach (Equation 11):

$$\check{\varsigma}=\frac{\sum_{\eta=1}^{r}\sum_{\zeta=1}^{r}\lambda_\eta\left(f\left(x\right)\right)\lambda_\zeta\left(f\left(x\right)\right)\left\{B_\eta^T\dot{x}-B_\eta{}^TA_\eta x(t)-\mu_{1\zeta}\left\|B_\eta\right\|^2u(t^-)\right\}}{\sum_{\eta=1}^{r}\sum_{\zeta=1}^{r}\lambda_\eta\left(f\left(x\right)\right)\lambda_\zeta\left(f\left(x\right)\right)\left\{\mu_{2\zeta}\left\|B_\eta\right\|^2\right\}} \quad (11)$$

It should be noted that this estimation is susceptible to measurement disturbances, as the use of a differentiator can amplify noise and degrade control performance. The estimation can be improved as shown in Equations 12 and 13 (for $\alpha_\eta>0$):

$$\dot{\hat{x}}=\sum_{\eta=1}^{r}\lambda_\eta\left(f\left(x\right)\right)\left\{-\alpha_\eta\hat{x}+\alpha_\eta B_\eta^Tx\right\} \quad (12)$$

$$\tilde{\varsigma}=\frac{\sum_{\eta=1}^{r}\sum_{\zeta=1}^{r}\lambda_\eta\left(f\left(x\right)\right)\lambda_\zeta\left(f\left(x\right)\right)\times\left\{\alpha_\eta\left(B_\eta^Tx-\hat{x}\right)-B_\eta{}^TA_\eta x-\mu_{1\zeta}\left\|B_\eta\right\|^2u\left(t^-\right)\right\}}{\sum_{\eta=1}^{r}\sum_{\zeta=1}^{r}\lambda_\eta\left(f\left(x\right)\right)\lambda_\zeta\left(f\left(x\right)\right)\left\{\mu_{2\zeta}\left\|B_\eta\right\|^2\right\}} \quad (13)$$

where $\hat{x}\in R$ is the state of a fuzzy low-pass filter and $\tilde{\varsigma}(t)$ is the estimation of ς. The basic estimating concept is similar to that given in a previous study.[13] In practice, since we know that

$$-\sum_{\zeta=1}^{\mathrm{r}}\lambda_{\zeta}\left(\mathrm{f}\left(\mathrm{x}\right)\right)\sqrt[\mathrm{r}]{\frac{1}{\beta_{\zeta}+\chi_{\zeta}}}\leq\varsigma\leq\sum_{\zeta=1}^{\mathrm{r}}\lambda_{\zeta}\left(\mathrm{f}\left(\mathrm{x}\right)\right)\sqrt[\mathrm{r}]{\frac{1}{\beta_{\zeta}+\chi_{\zeta}}}$$

when the estimated hysteresis state $\widetilde{\sigma}$ exceeds this allowable range, its value is clipped to the saturation value. That is, as proposed by Wu and Arunkumar,[13] the hysteresis state can be estimated using the following estimator (Equations 14 and 15):

$$\dot{\hat{x}}=\sum_{\eta=1}^{r}\lambda_{\eta}\left(f\left(x\right)\right)\left\{-\alpha_{\eta}\hat{x}+\alpha_{\eta}B_{\eta}^{T}x\right\} \tag{14}$$

$$\widehat{\varsigma}=\textstyle\sum_{\eta=1}^{r}\sum_{\zeta=1}^{r}\lambda_{\eta}\left(f\left(x\right)\right) \times\lambda_{\zeta}\left(f\left(x\right)\right)\ \left\{sat\left(\widetilde{\varsigma},\sqrt[r]{\frac{1}{\beta_{\zeta}+\chi_{\zeta}}}\right)\right\} \tag{15}$$

where *sat* denotes the saturation function, which is defined as follows

$$sat\left(h,\alpha\right)=\begin{cases}\alpha\cdot\operatorname{sgn}\left(h\right), & \text{if } |h|\geq\alpha\\ h, & \text{if } -\alpha<h<\alpha\end{cases}$$

Define the estimation error as $\varphi=\varsigma-\widehat{\varsigma}$, representing the difference between the actual hysteresis state ς and its estimate $\widehat{\varsigma}$ given in Equation 15. We can then reformulate Equation 8 in the following manner (Equations 16 and 17):

$$\dot{x}=\sum_{\eta=1}^{r}\sum_{\zeta=1}^{r}\lambda_{\eta}\left(f\left(x\right)\right)\lambda_{\zeta}\left(f\left(x\right)\right) \times\{A_{\eta}x+B_{\eta}(\mu_{1\zeta}u+\mu_{2\zeta}\widehat{\varsigma})+B_{\eta\zeta}\varphi\} \tag{16}$$

where $B_{\eta\zeta}=\mu_{2\zeta}B_{\eta}$ and let

$$u=\sum_{\zeta=1}^{r}\lambda_{\zeta}\left(f\left(x\right)\right)\left\{\frac{1}{\mu_{1\zeta}}\left(v-\mu_{2\zeta}\widehat{\varsigma}\right)\right\} \tag{17}$$

we have Equation 18:

$$\dot{x}=\sum_{\eta=1}^{r}\sum_{\zeta=1}^{r}\lambda_{\eta}\left(f\left(x\right)\right)\lambda_{\zeta}\left(f\left(x\right)\right)\left\{A_{\eta}x+B_{\eta}v+B_{\eta\zeta}\varphi\right\} \tag{18}$$

Note that $|\varphi|=|\varsigma-\widehat{\varsigma}|\leq2\sum_{\zeta=1}^{r}\lambda_{\zeta}\left(f\left(x\right)\right)\left\{\sqrt[r]{\frac{1}{\beta_{\zeta}+\chi_{\zeta}}}\right\}$ and therefore $\varphi\in L_{2}[0,t_{f}]$ for any $t_{f}>0$.

2.4. Design of fuzzy-based event-triggered non-fragile control scheme

To conserve limited resources and alleviate network bandwidth pressure, our study introduces an ET scheme, a highly effective strategy rooted in event protocols, designed to reduce transmissions of sampled data. Assuming the event generator is active, let $t_{k}h$ represent the latest transmission instant, and let the subsequent transmission instant $t_{k+1}h$ be (Equation 19):

$$t_{k+1}h=t_{k}h+\underset{s}{^{min}}\{sh|e^{T}\left(t_{k}h+sh\right)\Phi_{1}e\left(t_{k}h+sh\right) >\sigma x^{T}(t_{k}h)\Phi_{2}x(t_{k}h)\} \tag{19}$$

where $h>0$ denotes the sampling period, $0<\sigma<1$ represents known parameters, Φ_1,Φ_2 denote the positive definite matrices to be determined, and $e\left(t_{k}h+sh\right)=x\left(t_{k}h\right)-x\left(t_{k}h+sh\right)$ represents the deviation between the state at the previous transmission instant and that at the current sampling instant.

Based on the aforementioned trigger condition, we develop the following fuzzy non-fragile ET state feedback controller, defined by $\hat{v}\left(t\right)$, as follows (Equation 20):

Controller Rule ι: IF $f_1(x)$ *is* $F_{1\iota}$ and $f_2(x)$ *is* $F_{2\iota}$ and … and $f_q(x)$ *is* $F_{q\iota}$ THEN

$$\hat{v}(t)=\overline{K}_{\iota}(t)x\left(t_{k}h\right) \tag{20}$$

where $\overline{K}_{\iota}\left(t\right)=K_{\iota}+\Delta K_{\iota}\left(t\right)$, K_{ι} represent the state feedback gain matrix and $\Delta K_{\iota}\left(t\right)$ denotes a bounded gain variation in norms. In this context, we assume that the gain variation $\Delta K_{\iota}\left(t\right)$ follows the structure $\Delta K_{\iota}\left(t\right)=M_{\iota}F_{\iota}\left(t\right)N_{\iota}$, with M_{ι} and N_{ι} as established constant matrices and $F_{\iota}\left(t\right)$ represents an uncertain parameter matrix that complies with $F_{\iota}^{T}\left(t\right)F_{\iota}\left(t\right)\leq I$.

Then, the inferred output of the controller is expressed as Equation 21:

$$\hat{v}(t)=\sum_{\iota=1}^{r}\lambda_{\iota}\left(f\left(x\right)\right)\overline{K}_{\iota}(t)x\left(t_{k}h\right) \tag{21}$$

The holding interval of the zero-order hold, $\left[t_{k}h+\tau_{t_{k}},\ t_{k+1}h+\tau_{t_{k+1}}\right)$ is divided into subintervals, specifically (Equation 22)[17,20,21]:

$$\left[t_{k}h+\tau_{t_{k}},\ t_{k+1}h+\tau_{t_{k+1}}\right)=\bigcup_{s=0}^{t_{k+1}-t_{k}-1}T_{s} \tag{22}$$

where $T_{s}=[t_{k}h+sh+\tau_{t_{k}+s},\ t_{k}h+sh+h+\tau_{t_{k}+s+1}]$ for adequate $\tau_{t_{k}+s},\ s=0,\ldots,t_{k+1}-t_{k}$. The allowable network equivalent delay$\tau\left(t\right)$ is now defined as $\tau\left(t\right)=t-t_{k}h-sh,t\in T_{s}$. Then $0\leq\tau\left(t\right)\leq\overline{\tau}$.

In addition to that, following the earlier discussion, the modified control signal can be organized

in Equation 23:

$$\hat{v}(t)=\sum_{\iota=1}^{r}\lambda_{\iota}\left(f\left(x\left(t\right)\right)\right) \times\left\{\overline{K}_{\iota}\left(t\right)\left(x\left(t-\tau\left(t\right)\right)+e\left(t_{k}h\right)\right)\right\} \tag{23}$$

Then the closed-loop hysteresis control systems in Equation 1 can be presented as Equation 24 when combined with the controller design of Equation 23:

$$\begin{aligned}\dot{x}\left(t\right)=&\sum_{\eta=1}^{r}\sum_{\iota=1}^{r}\sum_{\zeta=1}^{r}\lambda_{\eta}\left(f\left(x\left(t\right)\right)\right)\lambda_{\iota}\\&\left(f\left(x\left(t\right)\right)\right)\lambda_{\zeta}\left(f\left(x\left(t\right)\right)\right)\\&\times\left\{A_{\eta}x\left(t\right)+B_{\eta}\overline{K}_{\iota}\left(t\right)\left(x\left(t-\tau\left(t\right)\right)+e\left(t_{k}h\right)\right)\right.\\&\left.+B_{\eta\zeta}\breve{\varphi}\left(t\right)\right\}\end{aligned} \tag{24}$$

where $\breve{\varphi}\left(t\right)=\varsigma\left(t\right)-\widehat{\varsigma}\left(t_{k}h\right)$ represents the updated estimation error.

Based on the ET scheme, the updated ideal controller for the hysteresis system in Equation 1 is structured in the following manner (Equation 25):

$$\begin{aligned}\tilde{u}\left(t\right)=&\sum_{\iota=1}^{r}\sum_{\zeta=1}^{r}\lambda_{\iota}\left(f\left(x\left(t\right)\right)\right)\lambda_{\zeta}\left(f\left(x\left(t\right)\right)\right)\\&\times\left\{\frac{1}{\mu_{1\zeta}}(\overline{K}_{\iota}(t)(x\left(t-\tau\left(t\right)\right)+e\left(t_{k}h\right))-\mu_{2\zeta}\widehat{\varsigma}\left(t_{k}h\right))\right\}\end{aligned} \tag{25}$$

Furthermore, the forthcoming assumption, definition, and lemma hold greater significance in supporting the necessary results in the upcoming section.

Assumption 1. Let $\vartheta>0$ be a given constant. The time-varying estimation error signal $\varphi\left(t\right)$ is assumed to satisfy $\int_{0}^{T_{f}}\varphi^{2}(t)dt\leq\vartheta$, and $[0,T_{f}]$ is a fixed FT interval.

Definition 1.[19] Given a time horizon T_{f}, the estimation error $\varphi\left(t\right)$ satisfying **Assumption 1**, the closed-loop T–S fuzzy B–W hysteresis control system in Equation 24 is defined as FTB with respect to $(\mathfrak{C}_{1},\ \mathfrak{C}_{2},\ T_{f},\ \vartheta,\ L)$ if

$$\begin{aligned}&\max_{s\in[-\overline{\tau},0]}\left\{\ x^{T}\left(s\right)Lx\left(s\right),\dot{x}^{T}\left(s\right)L\dot{x}\left(s\right)\right\}\leq\mathfrak{C}_{1}\\&\Longrightarrow x^{T}\left(t\right)Lx\left(t\right)<\mathfrak{C}_{2},t\in\left[0,T_{f}\right]\end{aligned} \tag{26}$$

where $L>0$ and $\mathfrak{C}_{2}>\mathfrak{C}_{1}>0$ (Equation 26).

Lemma 1.[22] Let $\tau(t)\in[0,\ \overline{\tau}]$, for any matrices $R,S\in\mathbb{R}^{n\times n}$ satisfying $\begin{bmatrix}R & *\\ S & R\end{bmatrix}>0$, the inequality below is guaranteed to hold:

$$-\overline{\tau}\int_{t-\overline{\tau}}^{t}\dot{x}^{T}\left(t\right)R\dot{x}\left(t\right)d\mathcal{X}\leq\Xi^{T}\left(t\right)\varrho\Xi\left(t\right)$$

where,

$$\Xi\left(t\right)=\begin{bmatrix}x\left(t\right)\\ x\left(t-\tau\left(t\right)\right)\\ x\left(t-\overline{\tau}\right)\end{bmatrix},$$

$$\varrho=\begin{bmatrix}-R & * & *\\ R^{T}-S^{T} & -2R+S+S^{T} & *\\ S^{T} & R^{T}-S^{T} & -R\end{bmatrix}$$

In this paper, our main objective is to develop an FT mixed $\mathcal{H}_{\infty}$ and a passivity control scheme for the T–S fuzzy B–W hysteresis control system in Equation 1, incorporating a novel ET non-fragile mechanism. We will specifically develop a non-fragile ET mixed $\mathcal{H}_{\infty}$ and a passivity controller to ensure that the closed-loop T–S fuzzy B–W hysteresis system in Equation 24 becomes FTB with respect to $(\mathfrak{C}_{1},\ \mathfrak{C}_{2},\ T_{f},\ \vartheta,\ L)$. The closed-loop system will also meet a specific performance index, indicated by the following inequality for a prescribed level of performance (Equation 27):

$$\begin{aligned}&\int_{0}^{T_{f}}\left\{\gamma^{-1}\theta z^{T}\left(t\right)z\left(t\right)-2\left(1-\theta\right)z^{T}(t)\varphi(t)\right\}dt\leq\gamma^{2}\\&\leq\gamma^{2}\int_{0}^{T_{f}}\varphi^{T}\left(t\right)\varphi\left(t\right)dt\end{aligned} \tag{27}$$

where $\theta\in[0,\ 1]$ acts as a parameter that balances the trade-off between $\mathcal{H}_{\infty}$ and passive performance.

3. Results

This section primarily aims to develop a novel T–S fuzzy ET non-fragile control scheme for B–W hysteresis control systems. More specifically, by leveraging the suitable Lyapunov–Krasovskii functional (LKF) and FT mixed $\mathcal{H}_{\infty}$ and passivity control metrics, we derived a novel set of sufficient criteria for the presence of T–S fuzzy ET non-fragile control designs with hysteresis behavior. These criteria are expressed in terms of LMIs and ensure that the closed-loop T–S fuzzy B–W hysteresis control systems in Equation 24 is FTB.

3.1. Finite-time boundedness analysis

In this subsection, we first analyze the FTB of T–S fuzzy B–W hysteresis control systems in Equation 24 under a non-fragile ET scheme.

Theorem 1. Let the trigger parameter $\sigma>0$, a nonnegative real scalar $\overline{\tau}$, the controller gain matrices K_{ι}, and the other parameters $\mu_{1\zeta},\ \mu_{2\zeta},\beta_{\zeta},\chi_{\zeta},\delta,\mathfrak{C}_{1}$ be given, then the closed-loop T–S fuzzy B–W hysteresis control system in Equation 24 with a non-fragile ET sampling scheme is FTB with respect to $(\mathfrak{C}_{1},\ \mathfrak{C}_{2},\ T_{f},\ \vartheta,\ L)$

if there exist symmetric positive definite matrices P, Q, R, Φ_1, Φ_2, an appropriately dimensioned matrix S, and scalars $\epsilon, \mathfrak{C}_2$ satisfying the following LMIs (Equations 28–30):

$$\aleph_{\eta\iota\zeta} = \begin{bmatrix} \aleph_1 & * & * & * \\ \aleph_s & -R^{-1} & * & * \\ 0 & \overline{\tau} M_\iota^T B_\eta^T & -\epsilon & * \\ \aleph_o & 0 & 0 & -\widetilde{\epsilon} \end{bmatrix} < 0 \tag{28}$$

$$\begin{bmatrix} R & * \\ S & R \end{bmatrix} > 0 \tag{29}$$

$$\mathfrak{C}_1 \ \Lambda + \vartheta \left(1 - e^{-\delta T_f}\right) < \Upsilon_1 \mathfrak{C}_2 \tag{30}$$

where

$$\aleph_1 = \begin{bmatrix} \aleph_{11} & * & * & * & * \\ \aleph_{21} & \aleph_{22} & * & * & * \\ \aleph_{31} & \aleph_{32} & \aleph_{33} & * & * \\ \aleph_{41} & 0 & 0 & \aleph_{44} & * \\ \aleph_{51} & 0 & 0 & 0 & \aleph_{55} \end{bmatrix},$$

$$\aleph_s = \left[\overline{\tau} A_\eta \ \overline{\tau} B_\eta K_\iota \ 0 \ \overline{\tau} B_\eta K_\iota \ \overline{\tau} B_{\eta\zeta} \right],$$

$$\aleph_o = \left[\aleph_{o_1} \ \aleph_{o_2} \ \aleph_{o_3} \right], \widetilde{\epsilon} = diag\left\{-\epsilon, -\epsilon, -\epsilon, -\epsilon\right\},$$

$$\aleph_{11} = Q + 2PA_\eta - R, \aleph_{21} = 2K_\iota^T B_\eta^T P^T + R - S,$$

$$\aleph_{22} = -2R + S + S^T + \sigma\Phi_2, \ \aleph_{31} = S,$$

$$\aleph_{32} = R - S,$$

$$\aleph_{33} = -Q - R, \ \aleph_{41} = 2K_\iota^T B_\eta^T P^T,$$

$$\aleph_{44} = -\Phi_1, \aleph_{51} = 2B_{\eta\zeta}^T P^T, \ \aleph_{55} = -\delta,$$

$$\aleph_{o_1} = \aleph_{o_3} = \left[0 \ \epsilon N_\iota \ 0 \ \epsilon N_\iota \ 0_{2n} \right],$$

$$\aleph_{o_2} = \left[M_\iota^T B_\iota^T P^T \ 0_{6n} \right].$$

Proof. Define the LKF candidate as follows (Equation 31):

$$V\left(x\left(t\right)\right) = x^T\left(t\right) P x\left(t\right) + \int_{t-\overline{\tau}}^{t} x^T\left(s\right) Q x\left(s\right) ds + \int_{t-\overline{\tau}}^{t} \int_{\theta}^{t} \dot{x}^T\left(s\right) R \dot{x}\left(s\right) ds d\theta \tag{31}$$

By computing the derivatives of $V\left(x\left(t\right)\right)$, we obtain Equation 32,

$$\dot{V}\left(x\left(t\right)\right) = 2x^T\left(t\right) P\dot{x}\left(t\right) + x^T\left(t\right) Q x\left(t\right) + \overline{\tau}^2 \dot{x}^T\left(t\right) R\dot{x}\left(t\right) - x^T\left(t-\overline{\tau}\right) Q x\left(t-\overline{\tau}\right) - \overline{\tau} \int_{t-\overline{\tau}}^{t} \dot{x}^T\left(s\right) R\dot{x}\left(s\right) ds \tag{32}$$

As per **Lemma 1**, the integral term in Equation 32 can be reformulated for any matrix S as follows (Equation 33):

$$-\overline{\tau} \int_{t-\overline{\tau}}^{t} \dot{x}^T\left(s\right) R\dot{x}\left(s\right) ds \leq \Xi^T\left(t\right) \overline{R} \Xi\left(t\right) \tag{33}$$

where,

$$\Xi\left(t\right) = \left[x^T\left(t\right) \ x^T\left(t - \tau\left(t\right)\right) \ x^T\left(t - \overline{\tau}\right) \right]^T,$$

$$\overline{R} = \begin{bmatrix} -R & * & * \\ R^T - S^T & -2R + S + S^T & * \\ S^T & R^T - S^T & -R \end{bmatrix}$$

Now, by unifying Equations 32 and 33 with Equation 19, and then applying the Schur complement, Equation 34 is obtained:

$$\begin{aligned} &\dot{V}\left(x\left(t\right)\right) - \delta V\left(x\left(t\right)\right) - \delta \breve{\varphi}^T\left(t\right) \breve{\varphi}\left(t\right) \\ &- e^T\left(i_k h\right) \Phi_1 e\left(i_k h\right) + \sigma x^T\left(t - \tau\left(t\right)\right) \Phi_2 x\left(t - \tau\left(t\right)\right) \\ &\leq \sum_{\eta=1}^{r} \sum_{\vartheta=1}^{r} \sum_{\zeta=1}^{r} \lambda_\eta\left(f\left(x\left(t\right)\right)\right) \lambda_\iota\left(f\left(x\left(t\right)\right)\right) \\ &\times \lambda_\zeta\left(f\left(x\left(t\right)\right)\right) \left[\psi^T\left(t\right) \aleph_{\eta\iota\zeta} \aleph \psi\left(t\right) \right] \end{aligned} \tag{34}$$

where,

$$\psi\left(t\right) = \left[x^T\left(t\right) \ x^T\left(t - \tau(t)\right) \ x^T\left(t - \overline{\tau}\right) \ e^T\left(i_k h\right) \ \breve{\varphi}^T\left(t\right) \right]^T$$

and the elements of $\aleph_{\eta\iota\zeta}$ are defined in Equation28. Hence, it can be inferred from Equation28 that $\aleph_{\eta\iota\zeta} < 0$. Consequently, we can derive Equation35:

$$\begin{aligned} &\dot{V}\left(x\left(t\right)\right) - \delta V\left(x\left(t\right)\right) - \delta \breve{\varphi}^T\left(t\right) \breve{\varphi}\left(t\right) < 0 \ or \\ &\frac{d}{dt}\left[e^{-\delta t} V\left(x\left(t\right)\right) \right] < \delta e^{-\delta t} \breve{\varphi}^T\left(t\right) \breve{\varphi}\left(t\right) \end{aligned} \tag{35}$$

Upon integrating the above inequality from 0 to t, where t belongs to the interval with $[0, T_f]$, it can be deduced that,

$$e^{-\delta T_f} V\left(x\left(t\right)\right) < V\left(x\left(0\right)\right) + \delta \int_0^{T_f} e^{-\delta T_f} \breve{\varphi}^T\left(s\right) \breve{\varphi}\left(s\right) ds.$$

Therefore, Equation 36 is derived:

$$V\left(x\left(t\right)\right) < e^{\delta T_f} \left[V\left(x\left(0\right)\right) + \vartheta(1 - e^{-\delta T_f}) \right] \tag{36}$$

By employing the transformations $\breve{P} = L^{-\frac{1}{2}} P L^{-\frac{1}{2}}$, $\breve{Q} = L^{-\frac{1}{2}} Q L^{-\frac{1}{2}}$, $\breve{R} = L^{-\frac{1}{2}} R L^{-\frac{1}{2}}$, Equation 37 can be computed:

$$\begin{aligned} &V\left(x\left(t\right)\right) \geq x^T\left(t\right) P x\left(t\right) = x^T\left(t\right) L^{\frac{1}{2}} \breve{P} L^{\frac{1}{2}} x\left(t\right) \\ &\geq \Upsilon_{\min}(\breve{\mathcal{P}}) x^T\left(t\right) L x\left(t\right) = \Upsilon_1 x^T\left(t\right) L x \end{aligned} \tag{37}$$

where $\Upsilon_1 = \Upsilon_{\min}\left(P\right)$ is the minimal eigenvalue of P.

Conversely, Equation 38 follows:

$$\begin{aligned} &V\left(x\left(0\right)\right)=x^{T}\left(0\right)Px\left(0\right)+\int_{-\overline{\tau}}^{0}x^{T}\left(s\right)Qx\left(s\right)ds\\ &+\overline{\tau}\int_{-\overline{\tau}}^{0}\int_{\theta}^{0}\dot{x}^{T}\left(s\right)R\dot{x}\left(s\right)dsd\theta\\ &\leq\left(\Upsilon_{2}+\overline{\tau}\Upsilon_{3}+\frac{\overline{\tau}^{3}}{2}\Upsilon_{4}\right)\max_{s\in[-\overline{\tau},0]}\\ &\left\{x^{T}\left(s\right)Lx\left(s\right),\dot{x}^{T}\left(s\right)L\dot{x}\left(s\right)\right\}\\ &\leq\mathfrak{C}_{1}\ \Lambda \end{aligned} \tag{38}$$

where $\Upsilon_{2}=\Upsilon_{\max}\left(P\right),\Upsilon_{3}=\Upsilon_{\max}\left(Q\right),\Upsilon_{4}=\Upsilon_{\max}\left(R\right),\ \mathfrak{C}_{1}=\Upsilon_{2}+\overline{\tau}\Upsilon_{3}+\frac{\overline{\tau}^{3}}{2}\Upsilon_{4}$. By analyzing Equation 35 through Equation 38, we can readily ascertain Equation 39:

$$x^{T}\left(t\right)Lx\left(t\right)\leq\frac{V\left(x\left(t\right)\right)}{\Upsilon_{1}}\leq\frac{\mathfrak{C}_{1}\ \Lambda+\vartheta\left(1-e^{-\delta T_{f}}\right)}{\Upsilon_{1}}. \tag{39}$$

Therefore, given that the condition in Equation 30 is satisfied, it becomes apparent that $x^{T}\left(t\right)Lx\left(t\right)\leq\mathfrak{C}_{2},\ \forall t\in\left[0,\ T_{f}\right]$. Thus, in accordance with **Definition 1**, the closed-loop form of T–S fuzzy B–W hysteresis control systems in Equation 24 is established as FTB concerning $(\mathfrak{C}_{1},\ \mathfrak{C}_{2},\ T_{f},\ \vartheta,\ L)$. This completes the proof.

3.2. Finite-time mixed $\mathcal{H}_{\infty}$ and passivity control design

In this subsection, we elaborate on the results presented in **Theorem 1** by integrating the FT mixed $\mathfrak{H}_{\infty}$ and passivity control methodology. We establish a set of fundamental criteria designed to enhance the efficacy of FT mixed $\mathcal{H}_{\infty}$ and passivity control within the framework of closed-loop T–S fuzzy B–W hysteresis control systems in Equation 24, incorporating an ET non-fragile scheme.

Theorem 2. Let the trigger parameter $\sigma>0$, a nonnegative real scalar $\overline{\tau}$, and the other parameters $\mu_{1\zeta},\ \mu_{2\zeta},\beta_{\zeta},\chi_{\zeta},\gamma,\theta,\delta,\ \mathfrak{C}_{1}$ be given, then the T–S fuzzy B–W hysteresis control system in Equation 24 with a non-fragile ET sampling scheme is FTB with a desired mixed $\mathfrak{H}_{\infty}$ and passivity control performance with respect to $(\mathfrak{C}_{1},\ \mathfrak{C}_{2},\ \mathrm{T_f},\ \vartheta,\ L)$ if there exist symmetric positive definite matrices P, Q, R, Φ_{1},Φ_{2}, appropriate dimensioned matrices S, Y_{ι}, and scalars $\epsilon,\mathfrak{C}_{2}$ satisfying the following LMIs (Equations 40–42):

$$\widetilde{\aleph}_{\eta\iota\zeta}=\begin{bmatrix}\widetilde{\aleph}_{1} & * & * & * & *\\ \widetilde{\aleph}_{s} & -2\kappa\mathrm{P}+\kappa^{2}\mathrm{R} & * & * & *\\ \widetilde{\aleph}_{h} & 0 & \widetilde{\aleph}_{77} & * & *\\ 0 & \overline{\tau}\mathrm{M}_{\iota}^{\mathrm{T}}\mathrm{B}_{\eta}^{\mathrm{T}}\mathrm{P} & 0 & -\epsilon & *\\ \widetilde{\aleph}_{o} & 0 & 0 & 0 & -\widetilde{\epsilon}\end{bmatrix}<0 \tag{40}$$

$$\begin{bmatrix}\mathrm{R} & *\\ \mathrm{S} & \mathrm{R}\end{bmatrix}>0 \tag{41}$$

$$\mathfrak{C}_{1}\ \Lambda+\vartheta\left(1-\mathrm{e}^{-\delta\mathrm{T_f}}\right)<\Upsilon_{1}\mathfrak{C}_{2} \tag{42}$$

where

$$\widetilde{\aleph}_{1}=\begin{bmatrix}\widetilde{\aleph}_{11} & * & * & * & *\\ \widetilde{\aleph}_{21} & \widetilde{\aleph}_{22} & * & * & *\\ \widetilde{\aleph}_{31} & \widetilde{\aleph}_{32} & \widetilde{\aleph}_{33} & * & *\\ \widetilde{\aleph}_{41} & 0 & 0 & \widetilde{\aleph}_{44} & *\\ \widetilde{\aleph}_{51} & 0 & 0 & 0 & \widetilde{\aleph}_{55}\end{bmatrix},$$

$$\widetilde{\aleph}_{s}=\begin{bmatrix}\overline{\tau}\mathrm{PA}_{\eta} & \overline{\tau}\mathrm{B}_{\eta}\mathrm{Y}_{\iota} & 0 & \overline{\tau}\mathrm{B}_{\eta}\mathrm{Y}_{\iota} & \overline{\tau}\mathrm{PB}_{\eta\zeta}\end{bmatrix},$$

$$\widetilde{\aleph}_{h}=\begin{bmatrix}\sqrt{\theta}\mathrm{D}_{\eta} & 0_{4n}\end{bmatrix},\quad \widetilde{\aleph}_{o}=\begin{bmatrix}\widetilde{\aleph}_{o_1} & \widetilde{\aleph}_{o_2} & \widetilde{\aleph}_{o_3}\end{bmatrix},$$

$$\widetilde{\epsilon}=\mathrm{diag}\left\{-\epsilon,-\epsilon,-\epsilon,-\epsilon\right\},\quad \widetilde{\aleph}_{11}=\mathrm{Q}+2\mathrm{PA}_{\eta}-\mathrm{R},$$

$$\widetilde{\aleph}_{21}=2\mathrm{Y}_{\iota}^{\mathrm{T}}\mathrm{B}_{\eta}^{\mathrm{T}}+\mathrm{R}-\mathrm{S},$$

$$\widetilde{\aleph}_{22}=-2\mathrm{R}+\mathrm{S}+\mathrm{S}^{\mathrm{T}}+\sigma\Phi_{2},\quad \widetilde{\aleph}_{31}=\mathrm{S},$$

$$\widetilde{\aleph}_{32}=\mathrm{R}-\mathrm{S},\ \widetilde{\aleph}_{33}=-\mathrm{Q}-\mathrm{R},\ \widetilde{\aleph}_{41}=2\mathrm{Y}_{\iota}^{\mathrm{T}}\mathrm{B}_{\eta}^{\mathrm{T}},$$

$$\widetilde{\aleph}_{44}=-\Phi_{1},\quad \widetilde{\aleph}_{51}=2\mathrm{B}_{\eta\zeta}^{\mathrm{T}}\mathrm{P}^{\mathrm{T}}-2\left(1-\theta\right)\mathrm{D}_{\eta},$$

$$\widetilde{\aleph}_{55}=-\gamma,\quad \widetilde{\aleph}_{77}=-\gamma,$$

$$\widetilde{\aleph}_{o_1}=\widetilde{\aleph}_{o_3}=\begin{bmatrix}0 & \epsilon\mathrm{N}_{\iota} & 0 & \epsilon\mathrm{N}_{\iota} & 0_{2n}\end{bmatrix},\quad \widetilde{\aleph}_{o_2}=\begin{bmatrix}\mathrm{M}_{\iota}^{\mathrm{T}}\mathrm{B}_{\eta}^{\mathrm{T}}\mathrm{P}^{\mathrm{T}} & 0_{6n}\end{bmatrix}$$

In addition, the required controller gain matrix is computed by $\mathrm{K}_{\iota}=\mathfrak{U}\mathfrak{W}^{-1}\mathrm{P}_{1}^{-1}\mathfrak{W}\mathfrak{U}^{\mathrm{T}}\mathrm{Y}_{\iota}$.

Proof. The establishment of the FTB property of closed-loop T–S fuzzy B–W hysteresis control systems in Equation 24 is evidenced by **Theorem 1**. We illustrate the FT mixed $\mathcal{H}_{\infty}$ and passivity control performance of the closed-loop T–S fuzzy B–W hysteresis control systems in Equation 24 under zero initial condition. Utilizing the same LKF used in **Theorem 1** and applying the derivation and the equation from Equation 27, Equation 43 can be calculated:

$$\begin{aligned} &\dot{V}\left(x\left(t\right)\right)-\delta V\left(x\left(t\right)\right)+\gamma^{-1}\theta z^{T}\left(t\right)z\left(t\right)\\ &-2\left(1-\theta\right)z^{T}\left(t\right)\breve{\varphi}\left(t\right)-\gamma\breve{\varphi}^{T}\left(t\right)\breve{\varphi}\left(t\right)\leq\psi^{T}\left(t\right)\widetilde{\aleph}_{\eta\iota\zeta}\psi\left(t\right) \end{aligned} \tag{43}$$

where $\widetilde{\aleph}_{51}=2B_{\varphi\eta}^{T}P^{T}-2\left(1-\theta\right)D_{\eta},\quad \widetilde{\aleph}_{h}=\begin{bmatrix}\sqrt{\theta}D_{\eta} & 0_{4n}\end{bmatrix},$ $\widetilde{\aleph}_{55}=-\gamma,\ \widetilde{\aleph}_{77}=-\gamma,$ with the remaining elements of $\widetilde{\aleph}_{\eta\iota\zeta}$ are identical to those in $\aleph_{\eta\iota\zeta}$ specified in **Theorem 1**. Moreover, for any positive

scalar κ, as a result of $(R-\kappa P)\,R^{-1}(R-\kappa P)\geq 0$, we can derive that $-PR^{-1}P\leq -2\kappa P+\kappa^2 R$. Replace $-PR^{-1}P$ by $-2\kappa P+\kappa^2 R$, $PB_\eta K_\iota$ by $B_\eta P_1 K_\iota$ and define $Y_\iota=\left(\mathfrak{UW}^{-1}P_1\mathfrak{WU}^T\right)K_\iota$ in Equation 43. By pre- and post-multiplying Equation 43 with $diag\{I,I,I,\ I,I,P,I,I,I,\ I\}$ and its transpose, we can obtain the controller gain matrices. This process produces the corresponding LMI as stated in Equation 40. Hence, fulfilling LMI in Equation 40 signifies Equation 44:

$$\begin{aligned}&\dot{V}\left(x\left(t\right)\right)-\delta V\left(x\left(t\right)\right)+\gamma^{-1}\theta z^T\left(t\right)z\left(t\right)\\&-2(1-\theta)z^T\left(t\right)\breve{\varphi}\left(t\right)-\gamma\breve{\varphi}^T\left(t\right)\breve{\varphi}\left(t\right)\leq 0\end{aligned}\quad(44)$$

After calculations and applying the mentioned inequality across the interval $[0,\ T_f]$ using Equation 27, it can be shown that the closed-loop T–S fuzzy B–W hysteresis control systems in Equation 24 demonstrate FTB and attain FT mixed $\mathcal{H}_\infty$ and passivity control characteristics concerning parameters $(\mathfrak{C}_1,\ \mathfrak{C}_2,\ T_f,\ \vartheta,\ L)$. This serves as the conclusive proof of the theorem.

To highlight the advantages of the proposed theoretical framework, we derive the following corollary for the T–S fuzzy ET sampling scheme applied to the B–W hysteresis control system in Equation 24 without the non-fragile controller. In the absence of the non-fragile controller, the T–S fuzzy B–W hysteresis control system in Equation 24 under the ET sampling scheme can be expressed as Equation 45:

$$\begin{aligned}&\dot{x}\left(t\right)=\sum_{\eta=1}^{r}\sum_{\iota=1}^{r}\sum_{\zeta=1}^{r}\lambda_\eta\left(f\left(x\left(t\right)\right)\right)\lambda_\iota\left(f\left(x\left(t\right)\right)\right)\\&\times\lambda_\zeta\left(f\left(x\left(t\right)\right)\right)\\&\left\{A_\eta x\left(t\right)+B_\eta K_\iota\left(x\left(t-\tau\left(t\right)\right)+e\left(t_k h\right)\right)\right.\\&\left.+B_{\eta\zeta}\breve{\varphi}\left(t\right)\right\}\end{aligned}\quad(45)$$

Corollary 1: Let the trigger parameter $\sigma>0$, a nonnegative real scalar $\overline{\tau}$, and the other parameters $\mu_{1\zeta},\ \mu_{2\zeta},\beta_\zeta,\chi_\zeta,\gamma,\theta,\delta,\ \mathfrak{C}_1$ be given, then the T–S fuzzy B–W hysteresis control system in Equation 45 with ET sampling scheme is FTB with a desired mixed $\mathfrak{H}_\infty$ and passivity control performance with respect to $(\mathfrak{C}_1,\ \mathfrak{C}_2,\ \mathrm{T_f},\ \vartheta,\ L)$ if there exist symmetric positive definite matrices P, Q, R, Φ_1,Φ_2, appropriate dimensioned matrices S, Y_ι, and scalars $\mathfrak{C}_2$ satisfying the following LMIs (Equations 3.2–3.2):

$$\widetilde{\aleph}_{\eta\iota\zeta}=\begin{bmatrix}\widetilde{\aleph}_1 & * & *\\ \widetilde{\aleph}_s & -2\kappa\mathrm{P}+\kappa^2\mathrm{R} & *\\ \widetilde{\aleph}_h & 0 & \widetilde{\aleph}_{77}\end{bmatrix}<0\quad(45)$$

$$\begin{bmatrix}\mathrm{R} & *\\ \mathrm{S} & \mathrm{R}\end{bmatrix}>0\quad(45)$$

$$\mathfrak{C}_1\Lambda+\vartheta\left(1-\mathrm{e}^{-\delta\mathrm{T_f}}\right)<\Upsilon_1\mathfrak{C}_2\quad(45)$$

where

$$\widetilde{\aleph}_1=\begin{bmatrix}\widetilde{\aleph}_{11} & * & * & * & *\\ \widetilde{\aleph}_{21} & \widetilde{\aleph}_{22} & * & * & *\\ \widetilde{\aleph}_{31} & \widetilde{\aleph}_{32} & \widetilde{\aleph}_{33} & * & *\\ \widetilde{\aleph}_{41} & 0 & 0 & \widetilde{\aleph}_{44} & *\\ \widetilde{\aleph}_{51} & 0 & 0 & 0 & \widetilde{\aleph}_{55}\end{bmatrix},$$

$$\widetilde{\aleph}_s=\left[\,\overline{\tau}\mathrm{PA}_\eta\ \overline{\tau}\mathrm{B}_\eta\mathrm{Y}_\iota\ 0\ \overline{\tau}\mathrm{B}_\eta\mathrm{Y}_\iota\ \overline{\tau}\mathrm{PB}_{\eta\zeta}\,\right],$$

$$\widetilde{\aleph}_h=\left[\,\sqrt{\theta}\mathrm{D}_\eta\ \ 0_{4\mathrm{n}}\,\right],$$

$$\widetilde{\aleph}_{11}=\mathrm{Q}+2\mathrm{PA}_\eta-\mathrm{R},\ \ \widetilde{\aleph}_{21}=2\mathrm{Y}_\iota^{\mathrm{T}}\mathrm{B}_\eta^{\mathrm{T}}+\mathrm{R}-\mathrm{S},$$

$$\widetilde{\aleph}_{22}=-2\mathrm{R}+\mathrm{S}+\mathrm{S}^{\mathrm{T}}+\sigma\Phi_2,\quad\widetilde{\aleph}_{31}=\mathrm{S},$$

$$\widetilde{\aleph}_{32}=\mathrm{R}-\mathrm{S},\ \ \widetilde{\aleph}_{33}=-\mathrm{Q}-\mathrm{R},\ \ \widetilde{\aleph}_{41}=2\mathrm{Y}_\iota^{\mathrm{T}}\mathrm{B}_\eta^{\mathrm{T}},$$

$$\widetilde{\aleph}_{44}=-\Phi_1,\quad\widetilde{\aleph}_{51}=2\mathrm{B}_{\eta\zeta}^{\mathrm{T}}\mathrm{P}^{\mathrm{T}}-2\left(1-\theta\right)\mathrm{D}_\eta,$$

$$\widetilde{\aleph}_{55}=-\gamma,\quad\widetilde{\aleph}_{77}=-\gamma$$

In addition, the required controller gain matrix is computed by $\mathrm{K}_\iota=\mathfrak{UW}^{-1}\mathrm{P}_1^{-1}\mathfrak{WU}^{\mathrm{T}}\mathrm{Y}_\iota$.

Remark 1: The hysteresis control approaches in previous studies mainly focus on classical force control, FT stabilization, or model predictive control for B–W hysteresis systems in **continuous-time control frameworks**.[10–12] These methods assume ideal controller implementation and continuous communication. In contrast, our study introduces a **fuzzy ET control framework,** which significantly reduces communication burden and optimizes the utilization of network resources. The controllers in previous studies do not account for the fragility issue arising from controller-gain uncertainties or implementation inaccuracies.[10–12,24–26] Our proposed method explicitly incorporates **non-fragile controller gain perturbations** into the control design, ensuring that the closed-loop T–S fuzzy B–W hysteresis system remains **FTB** even under gain uncertainties. This feature is critical for real-world implementations but has not been addressed in prior studies. Furthermore, unlike previous studies that either assume full state availability or do not explicitly estimate the hysteresis internal state,[10–12,24–26] we develop a **novel T–S fuzzy hysteresis state estimator** to reconstruct the virtual B–W hysteresis state. This estimator enables accurate **compensation of hysteresis effects** in a networked control environment and significantly improves control performance.

4. Illustrative examples

This section demonstrates the significance and applicability of the theoretical findings presented earlier using three simulation examples. In the first case example, a nonlinear permanent magnet synchronous motor (PMSM) system for a wind turbine[35] is transformed into a linear subsystem by applying T–S fuzzy rules, utilizing a novel fuzzy hysteresis characterization. Subsequently, the second example involves the Duffing forced-oscillator system.[35,36] The third example considers the **Lorenz chaotic system**, formulated as a T–S fuzzy model, to demonstrate the effectiveness of the proposed results in comparison with existing methods. All the examples are analyzed and verified against the sufficient stability condition established in Theorem 2. The simulation results demonstrate that the derived hysteresis-based fuzzy controller improves the guaranteed performance but also ensures the FTB of the systems under consideration.

Example 1. This example demonstrates the effectiveness of the proposed hysteresis-based control scheme for a PMSM-driven wind energy conversion system. The dynamic behavior of PMSMs has attracted significant research interest owing to their high efficiency in wind energy systems, increased power density, and relatively low manufacturing cost in industrial applications. Consequently, several researchers have focused on analyzing the dynamical behavior of the PMSM model by investigating its stability properties, bifurcation phenomena, and the emergence of chaotic solutions.[35–37] In contrast to earlier works, this study presents a stability analysis of the nonlinear PMSM model using the T–S fuzzy approach, wherein the nonlinear dynamics are represented through a set of linearized subsystems. To validate the proposed sufficient conditions, a nonlinear PMSM model adapted from Shanmugam and Joo[38] is employed, as detailed in Equation 4:

$$\frac{di_d}{dt} = \frac{-R_s i_d + n_p \omega L_q i_q + H(u_d)}{L_d}$$

$$\frac{di_q}{dt} = \frac{-R_s i_q + n_p \omega L_d i_d + H(u_q)}{L_q} \tag{37}$$

$$\frac{d\nu}{dt} = \frac{n_p \left\{(L_d - L_q)\, i_d i_q + \Theta \mathrm{i_q}\right\} - \alpha\nu - T_L}{J}$$

where the parameters of the aforementioned model are summarized in **Table 1**. By subsequently employing the affine and time-scaling transformations described by Shanmugam and Joo,[38] Equation 4 is obtained:

Table 1. Symbolic representation in the permanent magnet synchronous motor model

Notations	Description
$\boldsymbol{L_d}$ and $\boldsymbol{L_q}$	The stator inductors on $\boldsymbol{d-q}$ axis
v	Rotor angular velocity
$\boldsymbol{i_d}$ and $\boldsymbol{i_q}$	$\boldsymbol{d-q}$ axis currents
$\boldsymbol{u_d}$ and $\boldsymbol{u_q}$	$\boldsymbol{d-q}$ axis voltages
Θ	The permanent magnet flux linkage
n_p	The number of pole pairs
J	The polar moment of inertia
T_L	The load torque
R_S	Stator resistance
α	Viscous friction coefficient

$$\dot{\boldsymbol{x}}_{\boldsymbol{1}}(\boldsymbol{t}) = -\frac{\boldsymbol{L_q}}{\boldsymbol{L_d}}\boldsymbol{x_1}(\boldsymbol{t}) + \boldsymbol{x_2}(\boldsymbol{t})\,\boldsymbol{x_3}(\boldsymbol{t}) + \widetilde{\boldsymbol{u}}_{\boldsymbol{d}}$$

$$\dot{\boldsymbol{x}}_{\boldsymbol{2}}(\boldsymbol{t}) = -\boldsymbol{x_2}(\boldsymbol{t}) - \boldsymbol{x_1}(\boldsymbol{t})\,\boldsymbol{x_3}(\boldsymbol{t}) + \overline{\boldsymbol{\gamma}}\boldsymbol{x_3}(\boldsymbol{t}) + \widetilde{\boldsymbol{u}}_{\boldsymbol{q}} \tag{37}$$

$$\dot{\boldsymbol{x}}_{\boldsymbol{3}}(\boldsymbol{t}) = \boldsymbol{\varrho}\left(\boldsymbol{x_2}(\boldsymbol{t}) - \boldsymbol{x_3}(\boldsymbol{t})\right) + \boldsymbol{\vartheta}\boldsymbol{x_1}(\boldsymbol{t})\,\boldsymbol{x_2}(\boldsymbol{t}) - \widetilde{\boldsymbol{T}}_{\boldsymbol{L}}$$

where

$$\overline{\boldsymbol{\gamma}} = \frac{\boldsymbol{n_p}\boldsymbol{\Theta}^{\boldsymbol{2}}}{\boldsymbol{R_s}\boldsymbol{\alpha}},\ \boldsymbol{\varrho} = \frac{\boldsymbol{L_q}\boldsymbol{\alpha}}{\boldsymbol{R_s}\boldsymbol{J}},\ \widetilde{\boldsymbol{u}}_{\boldsymbol{q}} = \frac{\boldsymbol{n_p}\boldsymbol{L_q}\boldsymbol{\Theta}\boldsymbol{u_q}}{\boldsymbol{R_s^2}\boldsymbol{\alpha}},$$

$$\widetilde{\boldsymbol{u}}_{\boldsymbol{d}} = \frac{\boldsymbol{n_p}\boldsymbol{L_q}\boldsymbol{\Theta}\boldsymbol{u_d}}{\boldsymbol{R_s^2}\boldsymbol{\alpha}},\ \boldsymbol{\vartheta} = \frac{\boldsymbol{L_q}\boldsymbol{\alpha}^{\boldsymbol{2}}(\boldsymbol{L_d} - \boldsymbol{L_q})}{\boldsymbol{L_d}\boldsymbol{J}\boldsymbol{n_p}\boldsymbol{\Theta}^{\boldsymbol{2}}},\ \widetilde{\boldsymbol{T}}_{\boldsymbol{L}} = \frac{\boldsymbol{L_q^2}\boldsymbol{T_L}}{\boldsymbol{R_s^2}\boldsymbol{J}},$$

$$\boldsymbol{n_p} = \boldsymbol{1},\ [\boldsymbol{x_1}\ \boldsymbol{x_2}\ \boldsymbol{x_3}]^{\boldsymbol{T}} = [\boldsymbol{i_d}\ \boldsymbol{i_q}\ \boldsymbol{\nu}]^{\boldsymbol{T}}$$

We analyze the scenario with a smooth air gap, assuming $L_d = L_q$, and consider the external inputs to be zero, i.e., $\tilde{u}_d = \tilde{u}_q = \tilde{T}_L = 0$. In this context, ϑ and $\overline{\gamma}$ denote positive constants. Define the state vector as $x = [x_1\ x_2\ x_3]^T$, and consider the hysteresis control input $H(u)$ to formulate the control strategy for the system in Equation 1 along the $d-q$ axes. Accordingly, the resulting dynamic model can be expressed as Equation 35[38]:

$$\begin{aligned}
&\dot{x}_1(t) = -x_1(t) + x_2(t)\,x_3(t) + H(u(t))\\
&\dot{\boldsymbol{x}}_{\boldsymbol{2}}(\boldsymbol{t}) = -\boldsymbol{x_2}(\boldsymbol{t}) + \overline{\boldsymbol{\gamma}}\boldsymbol{x_3}(\boldsymbol{t}) - \boldsymbol{x_1}(\boldsymbol{t})\,\boldsymbol{x_3}(\boldsymbol{t}) + \boldsymbol{H(u(t))}\\
&\dot{\boldsymbol{x}}_{\boldsymbol{3}}(\boldsymbol{t}) = \boldsymbol{\varrho}\left(\boldsymbol{x_2}(\boldsymbol{t}) - \boldsymbol{x_3}(\boldsymbol{t})\right)
\end{aligned} \tag{33}$$

Prior to analyzing the stability of the nonlinear PMSM model in Equation 35 within the T–S fuzzy framework, the dynamic description of the n-dimensional T–S fuzzy model is introduced as

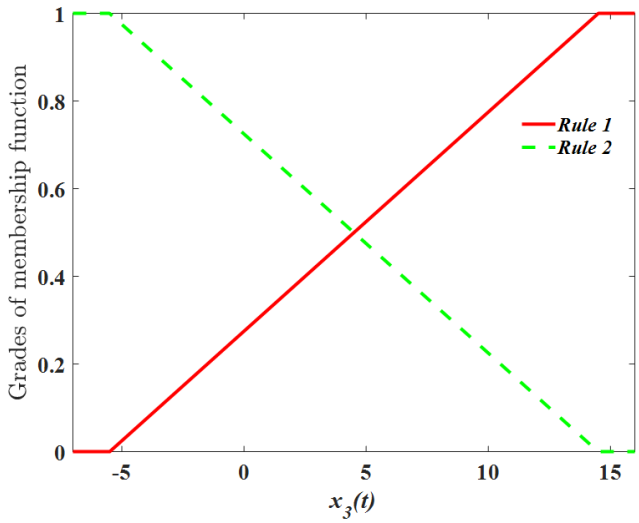

Figure 2. Membership function of the permanent magnet synchronous motor model

in Equation 34:

$$\dot{x} = \sum_{\eta=1}^{2}\sum_{\zeta=1}^{2} \lambda_\eta\left(f\left(x\left(t\right)\right)\right)\lambda_\zeta\left(f\left(x\left(t\right)\right)\right) \times\{A_\eta x\left(t\right) + B_\eta v\left(t\right) + B_{\eta\zeta}\varphi\left(t\right)\} \tag{33}$$

where

$$A_1 = \begin{bmatrix} -1 & c_1+d_1 & 0 \\ -(c_1+d_1) & -1 & \overline{\gamma} \\ 0 & \varrho & -\varrho \end{bmatrix},$$

$$A_2 = \begin{bmatrix} -1 & c_1+d_1 & 0 \\ -(c_1+d_1) & -1 & \overline{\gamma} \\ 0 & \varrho & -\varrho \end{bmatrix},$$

$$B_1 = B_2 = \begin{bmatrix} 1 \\ 1 \\ 0 \end{bmatrix}$$

where, $\varrho = 20$, $c_1 = 4.5$, $d_1 = 10$ and $\overline{\gamma} = 1.1$. Next, we consider the fuzzy membership functions following the approach in Ref. 38 as: $\lambda_1\left(f\left(x_3\right)\right) = \frac{1}{2}\left(1 - \frac{(c_1 - x_3)}{d_1}\right)$, $\lambda_2\left(f\left(x_3\right)\right) = 1 - \lambda_1\left(f\left(x_3\right)\right)$. Accordingly, the fuzzy membership functions for the T–S fuzzy model in Equation 34 are illustrated in **Figure 2**.

The B–W hysteresis model is defined by the parameter values μ_{11}= 0.7, μ_{12}= 0.8, μ_{21}= 0.3, μ_{22}= 0.2, β_1= 1.8, χ_1= 0.5,β_2= 1.9, χ_2= 0.7, and r= 2. Furthermore, the remaining matrices of the T–S fuzzy B–W hysteresis system in Equation 18 are selected as follows:

$$D_1 = \begin{bmatrix} 0.59 & 0.10 & 0.12 \end{bmatrix},$$

$$D_2 = \begin{bmatrix} 0.65 & 0.13 & 0.10 \end{bmatrix}, M_\iota = \begin{bmatrix} 0.2 & 0.1 & -0.1 \end{bmatrix}$$

$$N_1 = 0.19I,\ N_2 = 0.23I$$

For numerical simulation, the remaining parameters are chosen as follows:$\gamma = 0.9$, $\theta = 0.5$, $\alpha_1 = 1000$, $\alpha_2 = 1500$, $\sigma = 0.5$, $\mathfrak{C}_1 = 0.01$, $T_f = 5, \vartheta = 0.059, \kappa = 1$, $\mathcal{L} = I$, $\overline{\tau} = 0.1$.Utilizing the LMIs formulated in **Theorem 2**, the corresponding controller gain matrix is computed as follows:

$$K_1 = \begin{bmatrix} -0.0777 & -0.2017 & -0.0241 \end{bmatrix},$$

$$K_2 = \begin{bmatrix} -0.0327 & -0.3112 & -0.0451 \end{bmatrix}$$

Furthermore, we assume the initial condition as $x\left(0\right) = \begin{bmatrix} -0.4 & 0.4 & 0.2 \end{bmatrix}$. Utilizing these specified initial conditions in conjunction with the controller gain matrix, we evaluate the efficacy of the proposed approach through simulation results depicted in **Figures 3–7**. To briefly mention, **Figure 3A and 3B** illustrates the state trajectories of the T–S fuzzy B–W hysteresis system in Equation 24 with and without a controller. Additionally, **Figure 4A and 4B** depicts control signals corresponding to virtual and actual responses, as well as responses related to the estimation error of the hysteresis state. The figures depict the curves illustrating the instants and intervals of an ET release, along with error and threshold values in **Figure 5A and 5B**, respectively. Furthermore, **Figure 6A and 6B** depicts the time history $x^T\left(t\right)\ Lx(t)$ of the T–S fuzzy B–W hysteresis system. It is evident from **Figure 6A** that the B–W hysteresis system in Equation 24, with the proposed control, is FTB, as $x^T\left(t\right)\ Lx(t)$ remains below $\mathfrak{C}_2 = 0.7170$. Conversely, the time evolution of $x^T\left(t\right)\ Lx(t)$ without control is illustrated in **Figure 6B**, clearly indicating that the state exceeds the value of $\mathfrak{C}_2$. Therefore, it is evident that the proposed control maintains the system's stability. In **Figure 7A**,

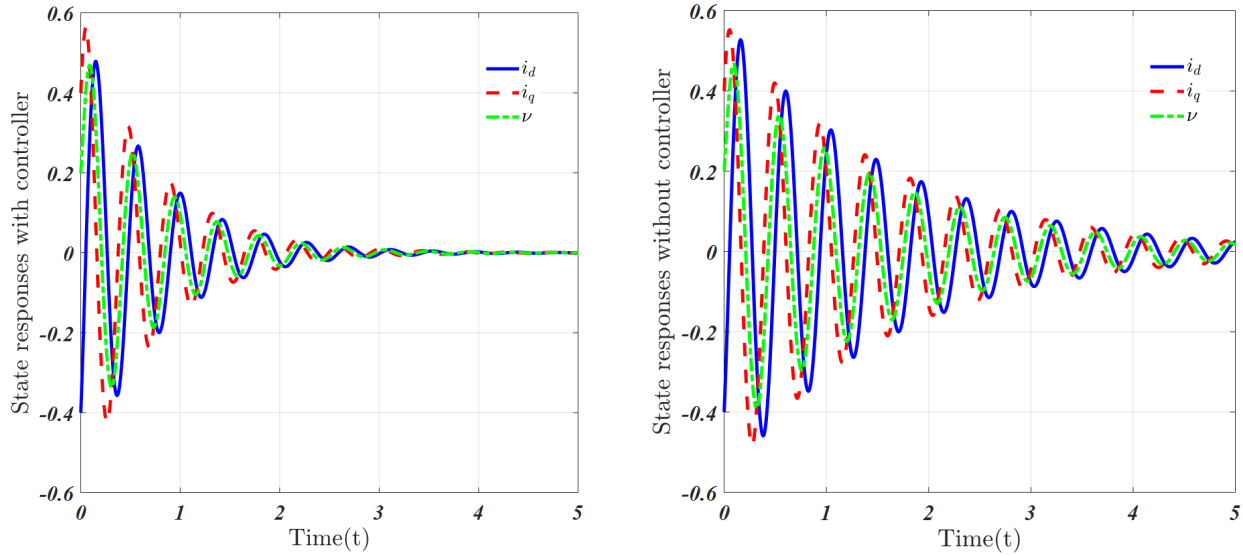

Figure 3. Simulation results of the (A) closed- and (B) open-loop Takagi–Sugeno fuzzy Bouc–Wen hysteresis system in Equation 24

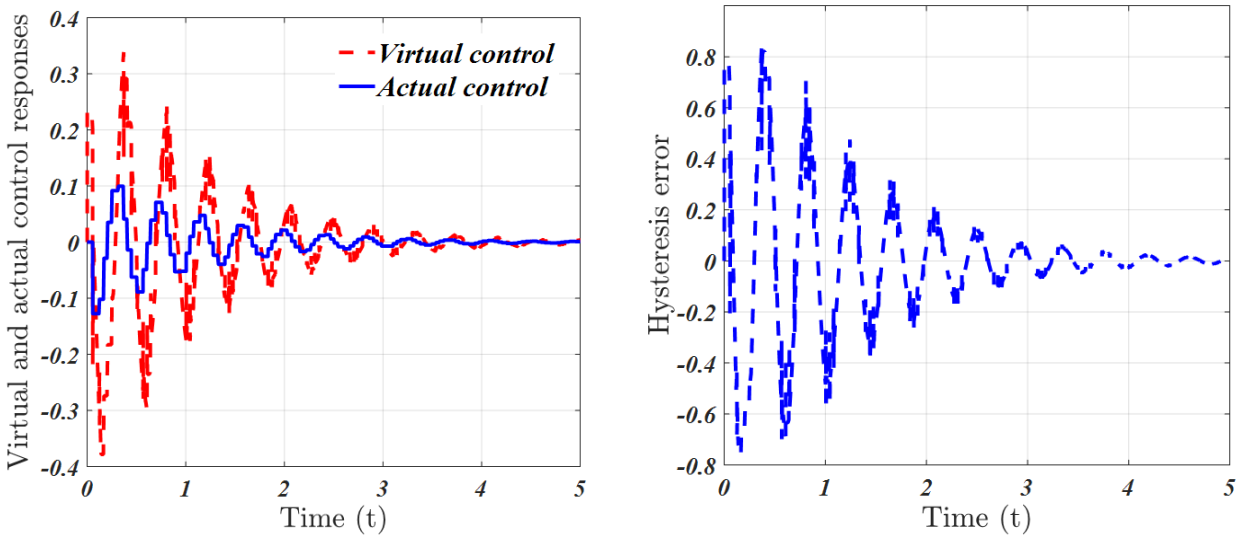

Figure 4. Results from simulating control responses under (A) virtual and (B) actual responses and the hysteresis error

the curve depicts the phase plot of the PMSM model in Equation 24 with control input, while **Figure 7B** illustrates the trajectories of the optimum bound value $\mathfrak{C}_2$ corresponding to different $\mathfrak{C}_1$. Additionally, **Tables 2 and 3** illustrate the calculated optimal value of $\mathfrak{C}_2$ for various combinations of $\mathfrak{C}_1$and $\bar{t}$. Furthermore, **Table 4** presents the calculated $\mathfrak{C}_2$ for different performances of θ. Overall, the simulation results reveal that the examined T–S fuzzy B–W hysteresis system in Equation 24 demonstrates FTB characteristics with respect to $(0.01,\ 0.7170,\ 5, 0.059,\ \mathrm{I})$, even when non-fragile occurrences arise in the system model.

Example 2. In this instance, the suggested control approach is implemented to ensure that the states of the Duffing forced-oscillation system[39,40] are made to track the states of a stable linear reference model operating within a networked environment. Take into account the following controlled plant with the hysteresis behavior (Equation 4)[39,40]:

$$\dot{x}_1(t) = x_2(t)$$

$$\dot{x}_2(t) = -x_1^3(t) - 0.1x_2(t) + H(u(t)) \qquad (25)$$

By considering that the state $\mathrm{x}_1(\mathrm{t}) \in [-5, 5]$, the system can be expressed using a T–S fuzzy model as in Equation 24, with the parameters

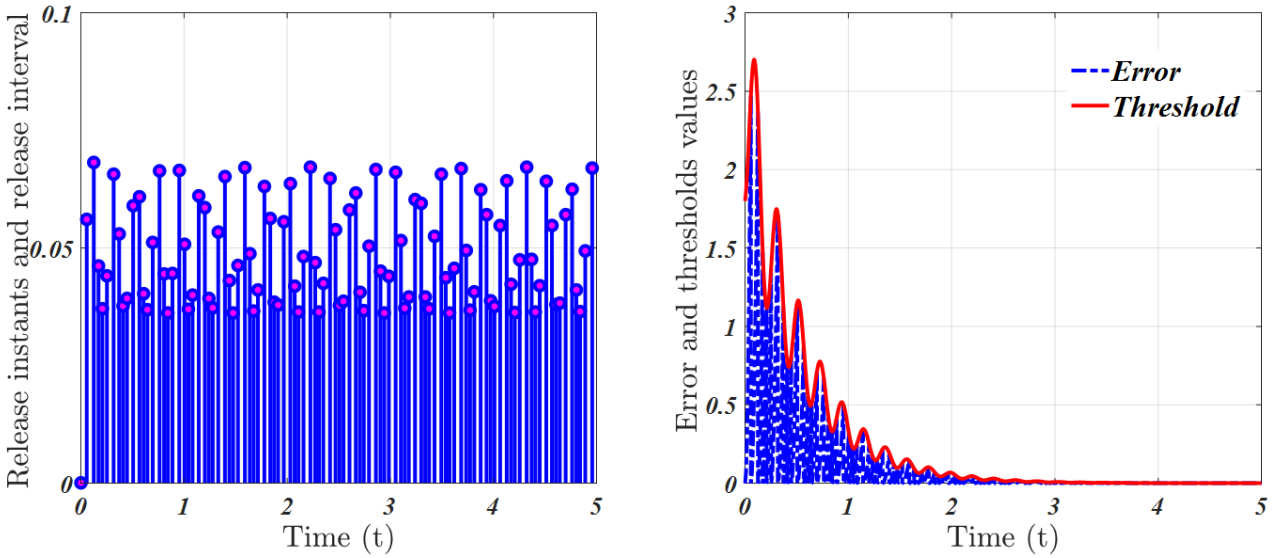

Figure 5. Responses of (A) release instants and release intervals, as well as the (B) error and thresholds for Takagi–Sugeno fuzzy Bouc–Wen hysteresis systems

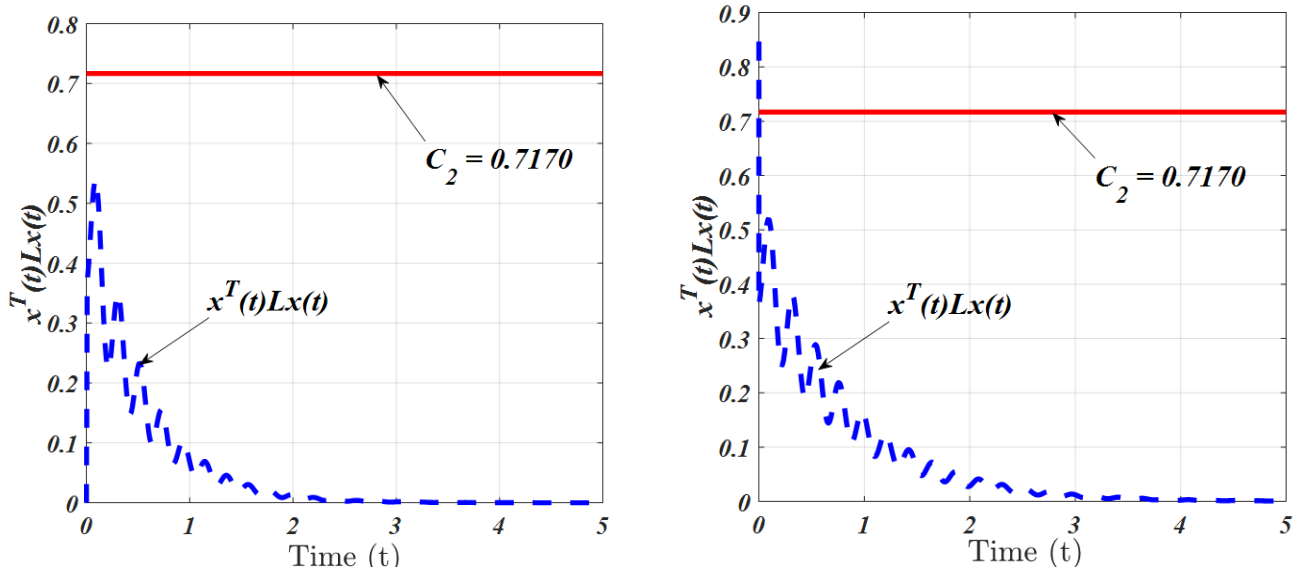

Figure 6. Evaluation $x^T(t)\,Lx(t)$ of (A) closed- and (B) open-loop Takagi–Sugeno fuzzy Bouc–Wen hysteresis system in Equation 24

Table 2. Optimum bound values of $\mathfrak{C}_2$ for various $\mathfrak{C}_1$

$\mathfrak{C}_1$	0.1	0.3	0.5	0.7	0.9	1.0
$\mathfrak{C}_2$	0.7170	1.4500	2.1831	2.9162	3.6492	4.0158

Table 3. Optimum bound values of $\mathfrak{C}_2$ for various $\overline{\tau}$

$\overline{\tau}$	0.01	0.02	0.03	0.04	0.05	0.10
$\mathfrak{C}_2$	0.5752	0.6025	0.6207	0.6656	0.7116	0.7170

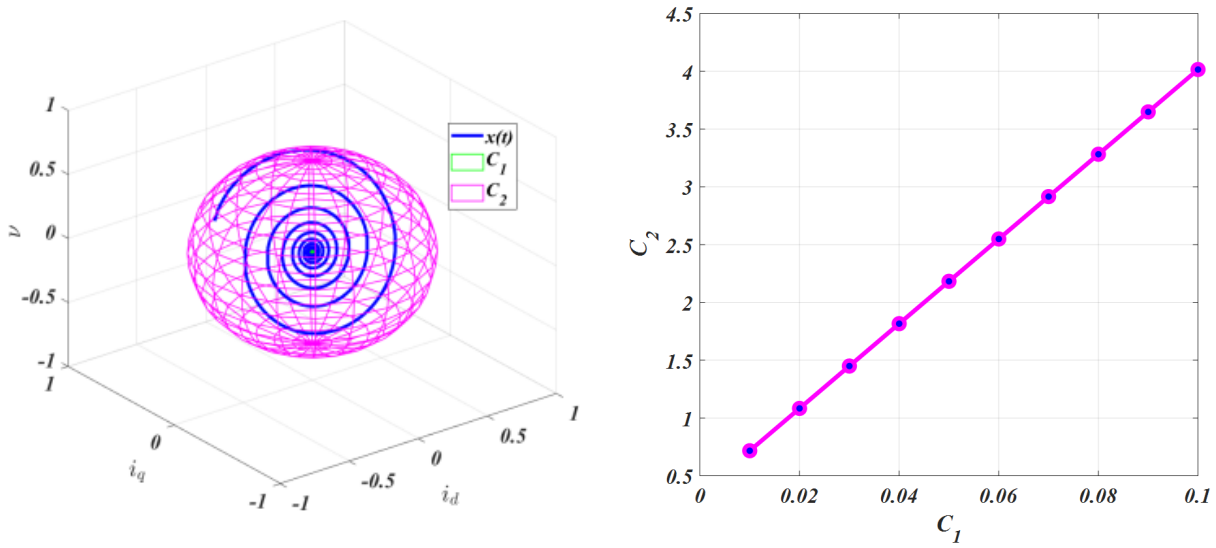

Figure 7. Simulation results of the PMSM model. (A) Phase plot of the PMSM model in Equation 24 with control input. (B) The relationship between $\mathfrak{C}_2$ and $\mathfrak{C}_1$

Table 4. Calculated $\mathfrak{C}_2$ for different performances

Performances	$\mathfrak{C}_2$
Passivity ($\theta = 0$)	0.7968
Mixed H_∞ and passivity ($\theta = 0.7$)	0.7170
$H_\infty(\theta = 1)$	0.9766

given below:

$$A_1=\begin{bmatrix}0 & 1\\ 0 & -0.1\end{bmatrix},\ A_2=\begin{bmatrix}0 & 1\\ -25 & -0.1\end{bmatrix},\ B_1=B_2=\begin{bmatrix}0\\ 1\end{bmatrix}$$

and we examine the fuzzy membership functions following the approach proposed by Gu et al.[39] as $\lambda_1(f(x_1)) = 1-\frac{x_1^2}{25},\ \ \lambda_2(f(x_1)) = 1-\lambda_1(f(x_1))$. Furthermore, the remaining matrices of the T–S fuzzy B–W hysteresis system in Equation 24 are selected as follows:

$$D_1 = \begin{bmatrix}0.51\ 0.12\end{bmatrix},\ D_2 = \begin{bmatrix}0.52\ 0.14\end{bmatrix},$$

$$M_\iota = \begin{bmatrix}0.2\ 0\end{bmatrix},\ N_1 = \begin{bmatrix}0.31 & 0\\ 0 & 0.22\end{bmatrix},$$

$$N_2 = \begin{bmatrix}0.33 & 0\\ 0 & 0.25\end{bmatrix}$$

The B–W hysteresis model retains the identical parameters, as in **Example (1)**. Moreover, the other parameters are selected as follows: as $\sigma = 0.5,\ \alpha_1 = 1000,\ \ \alpha_2 = 1500,\ \gamma = 0.9,\ \theta = 0.5,\ \kappa = 0.1,\ \mathfrak{C}_1 = 0.01,\ T_f = 5,\ \delta = 0.24,\ \overline{\tau} = 0.1,\ L = I,\ \vartheta = 0.089$. According to the parameter settings and the LMI feasibility conditions established in **Theorem 2**, we derive the following controller gain matrices:

$$K_1=\begin{bmatrix}-13.2961\ -6.8736\end{bmatrix},\ \ K_2=\begin{bmatrix}6.9444\ -2.9569\end{bmatrix}$$

The simulations are depicted sequentially using the aforementioned gain values and an initial condition $x(0) = \begin{bmatrix}0.4\ -0.4\end{bmatrix}$. Specifically, **Figure 8A and 8B** presents the simulation results of the open-loop and closed-loop T–S fuzzy B–W hysteresis system in Equation 24, respectively, including cases with an ET controller, an ET non-fragile controller, and without an ET non-fragile controller. From **Figure 8B**, it can be observed that the ET controller without non-fragility exhibits the fastest convergence, followed by the ET non-fragile controller with a slightly slower convergence rate, while the controller without the ET non-fragile mechanism converges the slowest. In contrast, the open-loop system fails to achieve convergence. Additionally, **Figure 9A and 9B** depicts the ET release instants and intervals, as well as error and threshold values for the T–S fuzzy B–W hysteresis system in Equation 24, respectively. The response curves for both the virtual and actual control signals and the estimation error of the hysteresis state are illustrated in **Figure 10A and 10B**. Additionally, the time history $x^T(t)\,Lx(t)$ of the closed- and open-loop T–S fuzzy B–W hysteresis system in Equation 24 is illustrated in **Figure 11A and 11B**. Furthermore, **Figure 12A and 12B** illustrates the state trajectories of the T–S fuzzy B–W hysteresis system in Equation 24 with and without control, respectively. It is evident from **Figures 11A and 12A** that the desired system in Equation 24 exhibits FTB behavior and does not exceed the

Table 5. Optimum bound values of $\mathfrak{C}_2$ for various $\mathfrak{C}_1$

C_1	**0.01**	**0.03**	**0.05**	**0.07**	**0.09**	**0.1**
Theorem 2	0.8918	2.4809	4.0700	5.6590	7.2481	8.0426
Corollary 1	0.9050	2.5059	4.1068	5.7077	7.3085	8.1090

Table 6. Optimum bound values of $\mathfrak{C}_2$ for various $\overline{\tau}$

$\overline{\tau}$	**0.01**	**0.03**	**0.07**	**0.1**	**0.13**	**0.15**
Theorem 2	0.4357	0.5043	0.6798	0.8918	1.0366	1.1834
Corollary 1	0.4433	0.6201	0.8244	0.9050	1.1791	1.2617

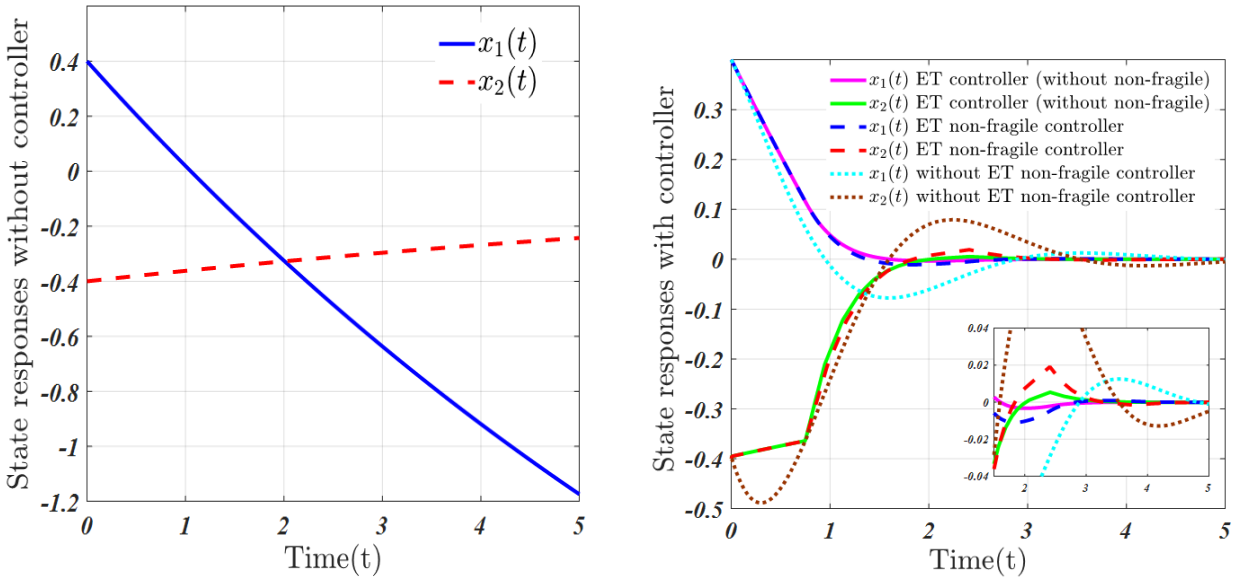

Figure 8. Simulation results of the T–S fuzzy B–W hysteresis system in Equation 24 showing the (A) open-loop case and (B) closed-loop cases with an event-triggered (ET) controller, an ET non-fragile controller, and without an ET non-fragile controller

bound $\mathfrak{C}_2 = 0.8918$. Additionally, **Tables 5 and 6** provide the calculated optimal bound values of $\mathfrak{C}_2$ for various $\mathfrak{C}_1$ and $\overline{\tau}$, for the cases with and without the non-fragile controller, respectively. The observed differences in the optimal $\mathfrak{C}_2$ bounds clearly demonstrate the influence of controller gain uncertainties on system performance. Therefore, it is confirmed that the ET-based non-fragile mechanism for T–S fuzzy B–W hysteresis system in Equation 24 is FTB with respect to $(0.01,\ 0.8918,\ 5, 0.089,\ \mathrm{I})$.

Example 3. To demonstrate the effectiveness of the proposed results in comparison with existing methods, we consider the Lorenz chaotic system formulated as a T–S fuzzy model. The Lorenz system is described as follows (Equation 23)[41,42]:

$$\dot{x}_1(t) = -ax_1(t) + a\,x_2(t) + H(u(t))$$

$$\dot{x}_2(t) = \mathrm{c}\,x_1(t) - x_2(t) - x_1(t)\,x_3(t)$$

$$\dot{x}_3(t) = x_1(t)\,x_2(t) - bx_3(t) \qquad (19)$$

where $x_1(t)$, $x_2(t)$ and $x_3(t)$ are the state variables, $H(u(t))$ denotes the control input with hysteresis behavior, while a, b, and c are the constants.

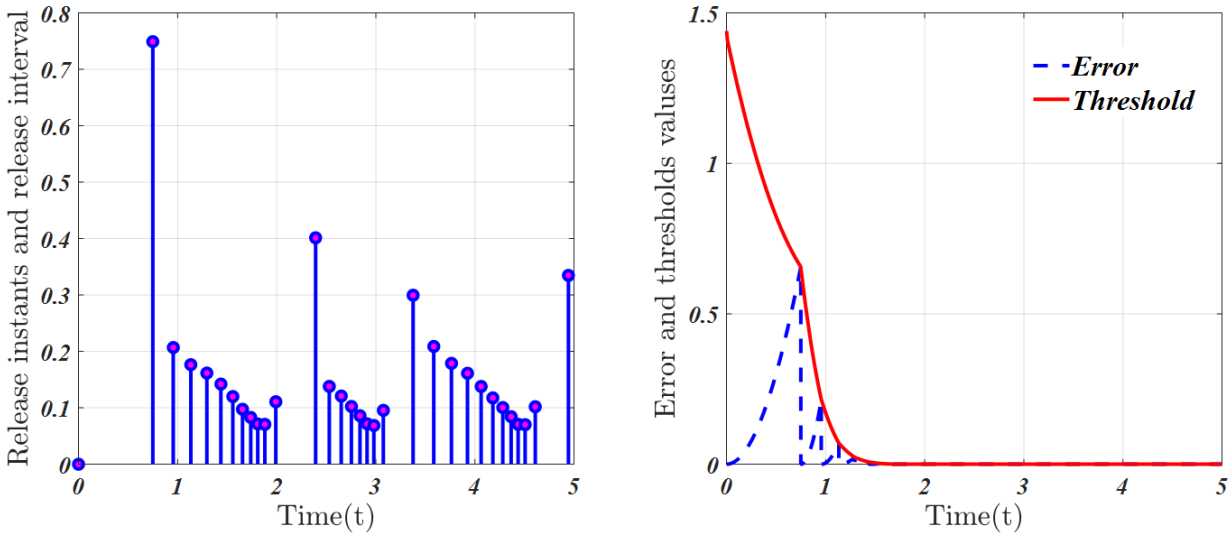

Figure 9. Responses of (A) release instants and release interval, as well as (B) error and thresholds for T–S fuzzy B–W hysteresis systems

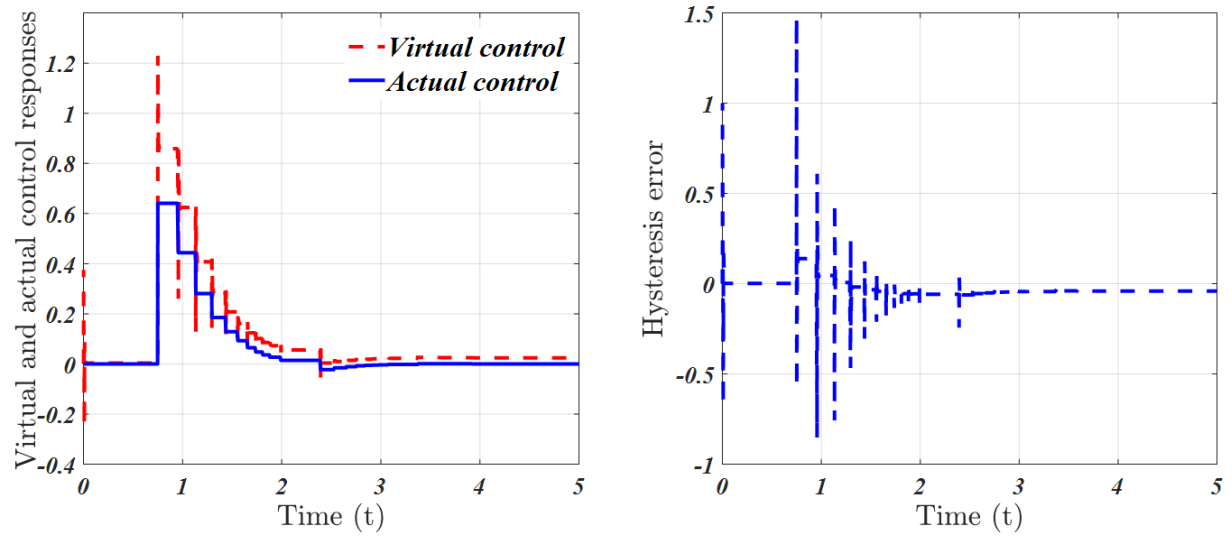

Figure 10. Results from simulating control responses under (A) virtual and actual responses and (B) the hysteresis error

Assuming that $x_1(t) \in [-d,\ d]$, the Lorenz system can be represented as the T–S fuzzy model with the following matrices[41,42]:

$$A_1=\begin{bmatrix} -a & a & 0 \\ c & -1 & -d \\ 0 & d & b \end{bmatrix},\ A_2=\begin{bmatrix} -a & a & 0 \\ c & -1 & d \\ 0 & d & b \end{bmatrix},\ B_1=B_2=\begin{bmatrix} 1 \\ 1 \\ 0 \end{bmatrix}$$

The system parameters are chosen as a = 10, b = 8/3, c = 28, and $d = 25$. The fuzzy membership functions are defined following the approach in previous studies as[41,42]:

$$\lambda_1(f(x_1)) = \frac{1}{2}\left(1+\frac{x_1}{d}\right),\ \lambda_2(f(x_1)) = 1-\lambda_1(f(x_1))$$

Furthermore, the B–W hysteresis model parameters and the remaining matrices are selected to be the same as those in **Example 1**. The remaining parameters of the T–S fuzzy B–W hysteresis system in Equation 24 are chosen $\gamma = 0.9$, $\theta = 0.5$, $\alpha_1 = 1000$, $\alpha_2 = 1500$, $\sigma = 0.5$, $\mathfrak{C}_1 = 0.01$, $T_f = 5$, $\vartheta = 0.059$, $\kappa = 0.01$, $L = I$. By solving the LMIs presented in **Theorem 2** for the T–S fuzzy B–W hysteresis Lorenz chaotic system, the maximum admissible delay upper bound $\overline{\tau}$ is obtained and summarized in **Table 7**. The results are compared to those reported in previous studies.[41,42] It can be observed from **Table 7** that the proposed approach provides significantly less conservative results than those in previous studies.[41,42]

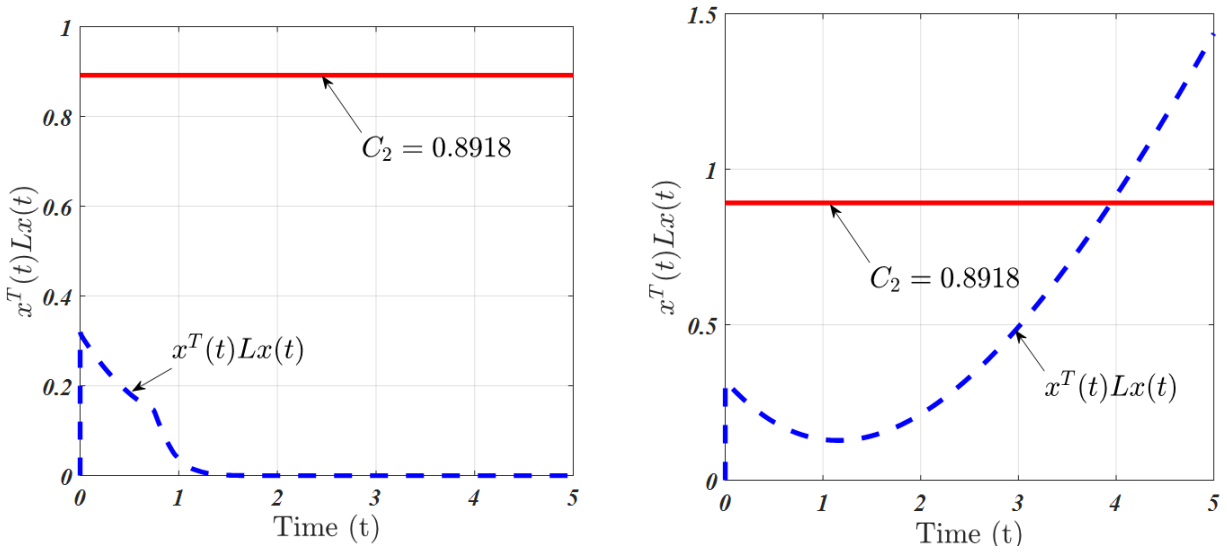

Figure 11. Evaluation $x^T(t)\,Lx(t)$ of the (A) closed- and (B) open-loop T–S fuzzy B–W hysteresis system in Equation 24

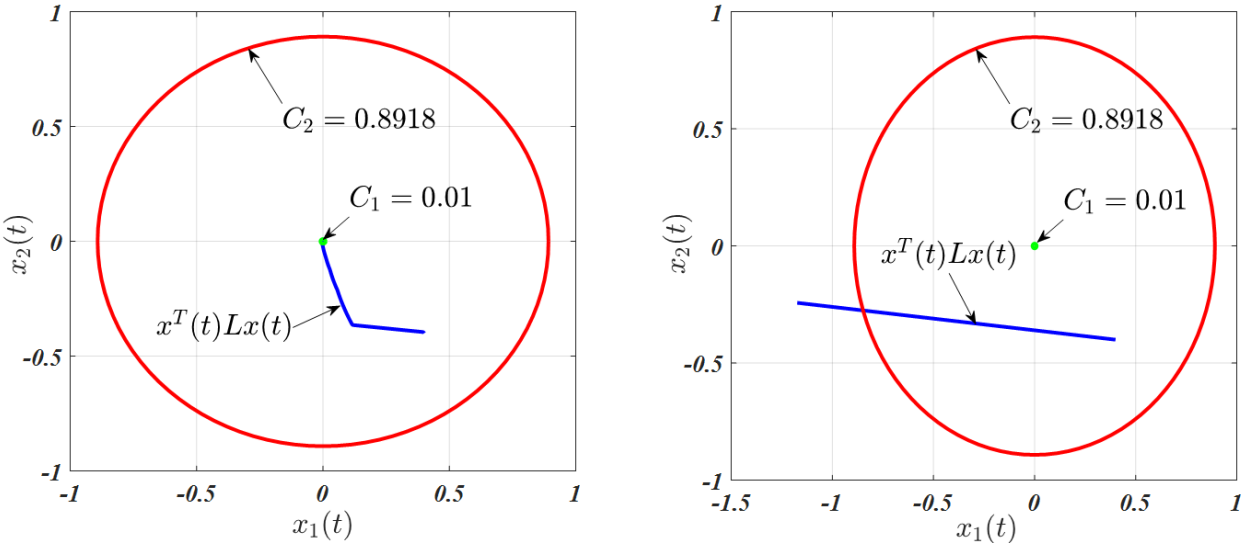

Figure 12. State behavior of the (A) closed- and (B) open-loop T–S fuzzy B–W hysteresis system in Equation 24

Table 7. Calculating the maximum bound of $\overline{\tau}$

Methods	Ref. 41	Ref. 42	Theorem 2
$\overline{\tau}$	0.0158	0.0299	0.0308

5. Conclusion

We introduced a novel hysteresis estimator-based non-fragile control scheme for a specific category of T–S fuzzy B–W hysteresis control systems, utilizing a fuzzy ET non-fragile mechanism approach. A precise model of the controlled system was employed to develop an innovative hysteresis-state estimator, capable of accurately estimating the hysteresis state. To address the issue of network communication load and to optimize the efficiency of network resource utilization, a fuzzy ET scheme was integrated. Additionally, this paper presents an innovative fuzzy control approach to designing hysteresis behavior, combining the ET mechanism with a non-fragile controller, thereby enhancing the robustness and efficiency of the control system. In summary, the proposed fuzzy controller effectively compensates for external disturbances by integrating FT mixed H_∞ and passivity conditions. This is achieved through the application of the LKF method combined with LMIs, leading to the formulation of a novel sufficient con-

dition that ensures the FTB of the closed-loop T–S fuzzy B–W hysteresis system with FT mixed H_∞ and passive performance. The theoretical results are substantiated, and their significance is demonstrated through three numerical examples, validating the practical applicability of the proposed approach. As a direction for future work, the interval type-2 fuzzy adaptive ET non-fragile control framework should be extended to nonlinear multi-agent systems with hysteresis behavior.

Acknowledgments

None.

Funding

This study is supported by the Ministry of Science and Technology of the Republic of China under grants: NSTC 110-2221-E-019-073-MY2, NSTC 110-2811-E-019-505-MY2, NSTC 114-2221-E-019-067 and NSTC 114-2811-E-019-004.

Conflict of interest

The authors declare that they have no conflict of interest regarding the publication of this article.

Author contributions

Conceptualization: Arumugam Arunkumar, Wen-Jer Chang, Jang-Lanq Wu
Formal analysis: Arumugam Arunkumar, Yann-Horng Lin
Investigation: All authors
Methodology: Arumugam Arunkumar, Yann-Horng Lin
Writing–original draft: All authors
Writing–review & editing: All authors

Availability of data

No datasets were generated or analyzed during the current study.

AI tools statement

All authors confirm that no AI tools were used in the preparation of this manuscript.

References

1. Tao G, Kokotovic PV. Adaptive control of plants with unknown hysteresis. *IEEE Trans Autom Control.* 1995;40(2):200-212. https://www.doi.org/10.1109/9.341778
2. Tan X, Baras JS. Modeling and control of hysteresis in magnetostrictive actuators. *Automatica.* 2004;40(9):1469-1480. https://www.doi.org/10.1016/j.automatica.2004.04.006
3. Su CY, Stepanenko Y, Svoboda J, Leung TP. Robust adaptive control of a class of nonlinear systems with unknown backlash-like hysteresis. *IEEE Trans Autom Control.* 2000;45(12):2427-2432. https://www.doi.org/10.1109/9.895588
4. Zhou J, Wen CY, Zhang Y. Adaptive backstepping control design of a class of uncertain nonlinear systems with unknown backlash-like hysteresis. *IEEE Trans Autom Control.* 2004;49(10):1751-1757. https://www.doi.org/10.1109/TAC.2004.835398
5. Mayergoyz ID. Vector Preisach models of hysteresis. In: *Mathematical Models of Hysteresis.* New York: Springer; 1991:141-201. https://www.doi.org/10.1007/978-1-4612-3028-1_3
6. Liu L, Tang L. Partial state constraints-based control for nonlinear systems with backlash-like hysteresis. *IEEE Trans Syst Man Cybern Syst.* 2018;50(8):3100-3104. https://www.doi.org/10.1109/TSMC.2018.2841063
7. Oh J, Drincic B, Bernstein DS. Nonlinear feedback models of hysteresis. *IEEE Control Syst. Mag.* 2009;29(1):100-119. https://www.doi.org/10.1109/MCS.2008.930919
8. Bouc R. Forced vibration of mechanical systems with hysteresis. In: *Proceedings of the 4th Conference on Nonlinear Oscillations, Prague, Czechoslovakia*; 1967: 315. https://cir.nii.ac.jp/crid/1570291225556669696
9. Wen YK. Method for random vibration of hysteretic systems. *ASCE J Eng Mech.* 1976;102(2):249-263. https://www.doi.org/10.1061/JMCEA3.0002106
10. Flores G, Rakotondrabe M. Classical Bouc–Wen hysteresis modeling and force control of a piezoelectric robotic hand manipulating a deformable object. *IEEE Control Syst Lett.* 2023;7:2413-2418. https://www.doi.org/10.1109/LCSYS.2023.3287142
11. Flores G, Rakotondrabe M. Finite-time stabilization of the generalized Bouc–Wen model for piezoelectric systems. *IEEE Control Syst Lett.* 2023;7:97-102. https://www.doi.org/10.1109/LCSYS.2022.3187127.
12. Flores G, Aldana N, Rakotondrabe M. Model predictive control based on the generalized Bouc-Wen model for piezoelectric actuators in robotic hand with only position measurements. *IEEE Control Syst Lett.* 2022;6:2186-2191. https://www.doi.org/10.1109/LCSYS.2021.3136456
13. Wu JL, Arunkumar A. Design of state-constrained controllers for Bouc–Wen hysteresis

systems. *IEEE Control Syst Lett.* 2023;7:3271-3276.
https://www.doi.org/10.1109/LCSYS.2023.3322097

14. Zhang Z, Xu S, Zhang B. Asymptotic tracking control of uncertain nonlinear systems with unknown actuator nonlinearity. *IEEE Trans Autom Control.* 2014;59(5):1336-1341.
https://www.doi.org/10.1109/TAC.2013.2289704
15. Zha L, Tian E, Xie X, Gu Z, Cao J. Decentralized event-triggered H_∞ control for neural networks subject to cyber-attacks. *Inf Sci.* 2018;457-458:141-155.
https://www.doi.org/10.1016/j.ins.2018.04.018
16. Xu B, Li YX. Prescribed-time fully distributed Nash equilibrium seeking of nonlinear multi-agent systems over unbalanced digraphs. *Automatica.* 2024;169:111847.
https://www.doi.org/10.1016/j.automatica.2024.111847
17. Arunkumar A, Wu JL. Observer-based disturbance rejection control for switched nonlinear networked systems under event-triggered scheme. In: *Disturbance Rejection Control*. IntechOpen; 2023.
https://www.doi.org/10.5772/intechopen.111434
18. Shi S, Fei Z, Karimi HR, Lam HK. Event-triggered control for switched T–S fuzzy systems with general asynchronism. *IEEE Trans Fuzzy Syst.* 2022;30(1):27-38.
https://www.doi.org/10.1109/TFUZZ.2020.3031027
19. Ren H, Zong G, Li T. Event-triggered finite-time control for networked switched linear systems with asynchronous switching. *IEEE Trans Syst Man Cybern Syst.* 2018;48(11):1874-1884.
https://www.doi.org/10.1109/TSMC.2017.2789186
20. Jhang JY, Wu JL, Yung CF. Design of event-triggered state constrained stabilizing controllers for nonlinear control systems. *IEEE Access.* 2022;10:3659-3667.
https://www.doi.org/10.1109/ACCESS.2021.3139963
21. Zhang CH, Yang GH. Event-triggered global finite-time control for a class of uncertain nonlinear systems. *IEEE Trans Autom Control.* 2020;65(3):1340-1347.
https://www.doi.org/10.1109/TAC.2019.2928767
22. Arunkumar A, Wu JL. Finite-time asynchronous event-triggered control for switched nonlinear cyber-physical systems with quantization. *IEEE Access.* 2023;11:135645-135658.
https://www.doi.org/10.1109/access.2023.3337814
23. Zong G, Ren H, Karimi HR. Event-triggered communication and annular finite-time H_∞ filtering for networked switched systems. *IEEE Trans Cybern.* 2021;51(1):309-317.
https://www.doi.org/10.1109/TCYB.2020.3010917
24. Liu Y, Arunkumar A, Sakthivel R, Alsaadi FE. Event-triggered non-fragile finite-time guaranteed cost control for uncertain switched nonlinear networked systems. *Nonlinear Anal Hybrid Syst.* 2020;36:100884.
https://www.doi.org/10.1016/j.nahs.2020.100884
25. Xu B, Li YX, Hou Z, Ahn AK. Dynamic event-triggered reinforcement learning-based consensus tracking of nonlinear multi-agent systems. *IEEE Trans Circuits Syst I Reg Pap.* 2023;70(5):2120-2132.
https://www.doi.org/10.1109/TCSI.2023.3246001
26. Guo S, Pan Y, Li H, Cao L. Dynamic event-driven ADP for N-player nonzero-sum games of constrained nonlinear systems. *IEEE Trans Autom Sci Eng.* 2024;22:7657-7669.
https://www.doi.org/10.1109/TASE.2024.3467382
27. Pan Y, Chen Y, Liang H. Event-triggered predefined-time control for full-state constrained nonlinear systems: a novel command filtering error compensation method. *Sci China Technol Sci.* 2024;67:2867-2880.
https://www.doi.org/10.1007/s11431-023-2607-8
28. Cao L, Ren H, Li H, Lu R. Event-triggered output-feedback control for large-scale systems with unknown hysteresis. *IEEE Trans Cybern.* 2021;51(11):5236-5247.
https://www.doi.org/10.1109/TCYB.2020.2997943
29. Liao X, Liu Z, Chen CLP, Zhang Y. Event-triggered fuzzy control for nonlinear time-delay system with full-state constraints and unknown hysteresis. *J Franklin Inst.* 2022;359(4):1582-1611.
https://www.doi.org/10.1016/j.jfranklin.2021.12.004
30. Son NN, Kien CV, Chinh TM. Event-triggered sliding mode control with hysteresis for motion tracking of piezoelectric actuated stage. *IEEE Access.* 2022;10:65309-65314.
https://www.doi.org/10.1109/ACCESS.2022.3183747
31. Ren C, He S, Luan X, Liu F, Karimi HR. Finite-time L_2 gain asynchronous control for continuous-time positive hidden Markov jump systems via T–S fuzzy model approach. *IEEE Trans Cybern.* 2020;51(1):77-87.
https://www.doi.org/10.1109/TCYB.2020.2996743
32. Aravindh D, Sakthivel R, Kavikumar R, Kaviarasan B, Robust finite-time non-fragile memory feedback control for uncertain systems

with external disturbance. *Int J Comput Math.* 2025;103(2):1-17. https://www.doi.org/10.1080/00207160.2025.2556115

33. Satheesh T, Kayalvizhi M, Sakthivel R, Sozhaeswari P. Finite-time secured non-fragile control design for engine throttle valve system with multiple attacks under proportional integral observer. Int J Robust Nonlinear Control. 2025;35(10):4201-4211. https://www.doi.org/10.1002/rnc.7897
34. Arunkumar A, Wu JL. Observer-based non-fragile event-triggered control of extra-corporeal blood circulation process in finite-time interval. *Int J Robust Nonlinear Control.* 2023;34;2141-2161. https://www.doi.org/10.1002/rnc.7074
35. Jing Z, Yu C, Chen G. Complex dynamics in a permanent magnet synchronous motor model. *Chaos Solitons Fract.* 2004;22(4):831-848. https://www.doi.org/10.1016/j.chaos.2004.02.054
36. Ouzaz M, Assoudi AE, Soulami J, Yaagoubi EHE. Simultaneous state and fault estimation for Takagi-Sugeno implicit models with Lipschitz constraints. *Int J Optim Control Theor Appl.* 2021;11(1):100-108. https://www.doi.org/10.11121/ijocta.01.2021.00877
37. Liu ZZ. Jin L, He Y. Sampling-fuzzy-dependent LKF for T–S fuzzy systems under sampled-data control. *IEEE Trans Fuzzy Syst.* 2025;33(10):3784-3794. https://www.doi.org/10.1109/TFUZZ.2025.3605340
38. Shanmugam L, Joo YH. Design of interval type-2 fuzzy-based sample data controller for nonlinear systems using novel fuzzy Lyapunov functional and its application to PMSM. *IEEE Trans Syst Man Cybern Syst.* 2021;51(1):542-551. https://www.doi.org/10.1109/TSMC.2018.2875098
39. Gu Z, Yue D, Lin J, Ding Z. H_∞ tracking control of nonlinear networked systems with a novel adaptive event-triggered communication scheme. *J Franklin Inst.* 2017;354:3540-3553. https://www.doi.org/10.1016/j.jfranklin.2017.02.020
40. Jia X, Zhang D, Hao X, Zheng N. Fuzzy H∞ tracking control for nonlinear networked control systems in T-S fuzzy model. *IEEE Trans Syst Man Cybern B Cybern.* 2009;39(4):1073-1079. https://www.doi.org/10.1109/TSMCB.2008.2010524
41. Lam HK, Leung FHF. Stabilization of chaotic systems using linear sampled-data controller. *Int J Bifurcat Chaos.* 2007;17(6):2021-2031. https://www.doi.org/10.1142/S0218127407018191
42. Zhu XL, Chen B, Yue D, Wang Y. An improved input delay approach to stabilization of fuzzy systems under variable sampling. *IEEE Trans Fuzzy Syst.* 2012;20(2):330-341. https://www.doi.org/10.1109/TFUZZ.2011.2174242

Arunkumar Arumugam *received the B.Sc., M.Sc., and M.Phil. Degrees in Mathematics from Bharathiar University, Coimbatore, India, in 2006, 2008, and 2009, respectively. He was awarded the Ph.D. Degree in Mathematics from Anna University, Chennai, India, in 2013. He was an Assistant Professor in Department of Mathematics, Karpagam Academy of Higher Education, Coimbatore, India from 2014 to 2016. He was a Post-Doctoral Research Fellow in the Department of Mathematics at Yangzhou University, China from 2017 to 2021. Currently, he is working as a Post-Doctoral Research Fellow in the Department of Marine Engineering, National Taiwan Ocean University, Keelung, Taiwan, ROC. To his credit, he has published more than 43 research papers in Science Citation Index journals. His current research interests include nonlinear networked systems, fuzzy control, marine engineering, state-constrained control and delay differential systems.*
https://orcid.org/0000-0001-8194-6364

Jenq-Lang Wu *(Member, IEEE) received his B.S. degree and Ph.D. degree in Electrical Engineering from National Taiwan University of Science and Technology, Taipei, Taiwan, in 1991 and 1996, respectively. He is currently a Professor with the Department of Electrical Engineering, National Taiwan Ocean University, Keelung, Taiwan. His current research interests include nonlinear control systems, state constrained control, structural-constrained controller design, and multi objective control. Dr. Wu is a recipient of the 2009 Ta-You Wu Memorial Award of the National Science Council of Taiwan.*
https://orcid.org/0000-0003-1621-3812

Wen-Jer Chang *received the M.S. Degree from the Institute of Computer Science and Electronic Engineering from the National Central University in 1990 and the Ph.D. Degree from the Institute of Electrical Engineering of the National Central University in 1995. Since 1995, he has been with the National Taiwan Ocean University, Keelung, Taiwan, ROC. He is currently a Distinguished Professor of the Department of Marine Engineering and the Director of the Center for Social Responsibility and Sustainable Development of National Taiwan Ocean University. In 2014 and 2022, he received the Outstanding Research Teacher Award from the National Taiwan Ocean University. From 2018 to 2023, he was a Member of the Council of the Taiwan Fuzzy Systems Association (TFSA). Since 2021, he has been the Chairman of the Association of Marine Affairs. From 2021 to 2023, he was a Member of the Council of the International Association of Electrical, Electronic, and Energy Engineering (IAEEEE). In 2022, he was*

elected to the grade of IEEE Senior Member. From 2021 to 2024, he is listed in the "World's Top 2% Scientists," according to Stanford University. He has authored more than 170 published journal papers and 150 refereed conference papers. His recent research interests are intelligent control, fuzzy control, robust control, marine engineering, and smart shipping.
https://orcid.org/0000-0001-5054-8451

Yann-Horng Lin *received his B.S. Degree from the Department of Marine Engineering of the National Taiwan Ocean University, Taiwan, ROC, in 2016. In 2018 and 2025, he received the M.S. Degree and Ph.D. Degree in Marine Engineering from the National Taiwan Ocean University. He received the best Doctoral Dissertation Award from the council of the Taiwan Fuzzy Systems Association (TFSA) in 2025. His recent research interests focus on type-2 fuzzy control, multi-agent control systems, performance-guaranteed control, formation and containment control, and intelligent control applications.*
https://orcid.org/0000-0002-4967-8299

An International Journal of Optimization and Control: Theories & Applications (https://accscience.com/journal/ijocta)